Chromosoma
https://doi.org/10.1007/s00412-022-00772-5

ORIGINAL ARTICLE

Kinesin-5 Eg5 mediates centrosome separation to control spindle assembly in spermatocytes

Zhen-Yu She[1,2] · Ning Zhong[1,2] · Ya-Lan Wei[3,4]

Received: 2 December 2021 / Revised: 12 March 2022 / Accepted: 8 April 2022

Abstract

Timely and accurate centrosome separation is critical for bipolar spindle organization and faithful chromosome segregation during cell division. Kinesin-5 Eg5 is essential for centrosome separation and spindle organization in somatic cells; however, the detailed functions and mechanisms of Eg5 in spermatocytes remain unclear. In this study, we show that Eg5 proteins are located at spindle microtubules and centrosomes in spermatocytes both in vivo and in vitro. We reveal that the spermatocytes are arrested at metaphase I in seminiferous tubules after Eg5 inhibition. Eg5 ablation results in cell cycle arrest, the formation of monopolar spindle, and chromosome misalignment in cultured GC-2 spd cells. Importantly, we find that the long-term inhibition of Eg5 results in an increased number of centrosomes and chromosomal instability in spermatocytes. Our findings indicate that Eg5 mediates centrosome separation to control spindle assembly and chromosome alignment in spermatocytes, which finally contribute to chromosome stability and faithful cell division of the spermatocytes.

Keywords Kinesin-5 · Eg5 · Spermatocytes · Centrosome · Microtubule · Spindle

Introduction

In eukaryotic cells, centrosomes are the key microtubule-organizing centers, which are crucial for spindle assembly and chromosome segregation in cell division (Bornens 2002). Centrosomes consist of a pair of centrioles and are separated to form the bipolar spindle at the G_2/M transition (Agircan et al. 2014; Hashimoto et al. 2020). The collaborations of microtubules, microtubule-associated proteins, and motor proteins are necessary for the assembly of the bipolar spindle during cell division (Yount et al. 2015; Yukawa et al. 2019).

Kinesin-5 motor is a conserved plus-end–directed motor required for the formation of the bipolar spindle (Sawin et al. 1992; Heck et al. 1993; Blangy et al. 1995; Mann and Wadsworth 2019). Kinesin-5 motors crosslink antiparallel microtubules, generate outward pushing force on centrosomes, and regulate centrosome separation (Kashina et al. 1996; Kapoor et al. 2000; Kapitein et al. 2005; Hentrich and Surrey 2010; Raaijmakers et al. 2012). In mammalian cells, kinesin-5 Eg5 generates braking forces (Shimamoto et al. 2015), regulates spindle cohesion and kinetochore fiber stability (Ma et al. 2011; Chen et al. 2018), and maintains spindle bipolarity (Gayek and Ohi 2014). Mutation or inhibition of Eg5 leads to defects in centrosome separation and the formation of the monopolar spindle in mitotic cells (Mayer et al. 1999; Ferenz et al. 2010).

The balances between kinesin-5 motors and the minus-end–directed motors, including dynein and kinesin-14 motors, are essential for bipolar spindle assembly (Cameron et al. 2006; Ferenz et al. 2010; Tanenbaum and Medema 2010; Gayek and Ohi 2014; van Heesbeen et al. 2014; Sturgill et al. 2016). Eg5 ablation results in mitotic spindle defects, the activation of spindle assembly checkpoint, and cell apoptosis (Mayer et al. 1999; Liu

Zhen-Yu She and Ning Zhong contributed equally to this work.

✉ Zhen-Yu She
zhenyushe@fjmu.edu.cn

1 Department of Cell Biology and Genetics, The School of Basic Medical Sciences, Fujian Medical University, Fuzhou 350122, Fujian, China

2 Key Laboratory of Stem Cell Engineering and Regenerative Medicine, Fujian Province University, Fuzhou 350122, Fujian, China

3 Fujian Obstetrics and Gynecology Hospital, Fuzhou 350011, Fujian, China

4 Medical Research Center, Fujian Maternity and Child Health Hospital, Affiliated Hospital of Fujian Medical University, Fuzhou 350001, Fujian, China

Published online: 18 April 2022

et al. 2014). Moreover, homozygous deletion of *Eg5* in mice leads to monopolar spindles, cell cycle arrest, and inhibited cell proliferation of early embryos prior to the implantation stage (Castillo and Justice 2007; Chauvière et al. 2008).

In meiosis, Eg5 is responsible for meiotic progression and spindle organization in porcine oocytes (Wan et al. 2018; Xie et al. 2018). Furthermore, the increased level of Eg5 proteins on meiosis II spindles is associated with the maintenance of the bipolar spindle in mouse oocytes (Kovacovicova et al. 2016). During meiosis, Eg5 proteins are expressed in spermatocytes in seminiferous tubules (Hara-Yokoyama et al. 2019). In our previous studies, Eg5 inhibition by specific inhibitors, including Monastrol, *S*-trityl-*L*-cysteine (STLC), and dimethylenastron, results in the defects in spindle bipolarity and chromosome misalignment in spermatocytes (She et al. 2020). STLC binds to the pocket composed of loop L5 and helix α2 and α3 in Eg5's motor domain and inhibits the release of ADP (DeBonis et al. 2004; Skoufias et al. 2006; Kaan et al. 2009). In mitotic cells, STLC-mediated Eg5 inactivation leads to the formation of monopolar spindles (Skoufias et al. 2006; Iwakiri et al. 2013; Novak et al. 2018). Despite the importance of Eg5 in meiosis, our understanding of the mechanisms of kinesin-5 Eg5 in dividing spermatocytes is still rudimentary. Therefore, it remains unclear how Eg5 mediates spindle bipolarity to regulate faithful chromosome alignment in spermatocytes.

Here, to fill this knowledge gap, we combine the in vivo inhibition of Eg5 in mouse testes with cultured spermatocytes to investigate the functions and mechanisms of Eg5 in the cell division of spermatocytes. The use of the GC-2 spd cells—the model cell widely used for studying spindle assembly of spermatocytes—allowed us to perform Eg5 knockdown/inhibition as well as immunofluorescence to visualize the organization and dynamics of spindle microtubules. We find that Eg5 inhibition results in cell cycle arrest of spermatocytes at metaphase I in seminiferous tubules. Furthermore, Eg5 ablation leads to the formation of the monopolar spindle, spindle disorganization, and chromosome misalignment in cultured spermatocytes. Furthermore, we demonstrate that Eg5 is responsible for the separation of centrosomes and the maintenance of spindle bipolarity, which finally contributes to the formation of bipolar spindle and chromosomal stability. Strikingly, the long-term inhibition of Eg5 in cultured spermatocyte results in significantly increased numbers of centrosomes and genome instability. Our data suggest that kinesin-5 Eg5 mediates centrosome separation to regulate spindle bipolarity and chromosome stability in spermatocytes.

Materials and methods

Mouse experiments and animal ethics

All animal experiments were reviewed and approved by the Institutional Animal Care and Use Committee at Fujian Medical University, China (Protocol No. SYXK2016-0007). All mouse experiments were performed according to the guidelines of the Care and Use of Laboratory Animals of the National Institutes of Health (NIH publications No. 8023, revised 1978).

The 3-week-old male ICR mice were purchased from the Wu-Shi experimental animal center (Fuzhou, China). The mice were fed and housed in a pathogen-free facility at Fujian Medical University under the standard environments and exposed to a 12:12-h light/dark cycle with free access to water and food. For Eg5 inhibition, the mice were treated with 21.34 mg/kg STLC (Santa Cruz Biotechnology, Cat. sc-202799) by intraperitoneal injection every 2 days for 2 weeks. The concentrations of STLC were selected according to previous studies (Brier et al. 2004; DeBonis et al. 2004; Gartner et al. 2005; Shimizu et al. 2010; She et al. 2020).

Cell culture, treatment, and transfection

The GC-2 spd (ts) cell line (ATCC No. CRL-2196) was purchased from American Type Culture Collection. Cells were cultured in Dulbecco Modified Eagle's Medium (DMEM)/high glucose, (HyClone, Cat. SH30022.01) supplemented with 10% heat-inactivated fetal bovine serum (Every green, Cat. 11011–8611) and 1% penicillin/streptomycin (MP Biomedicals, Cat. 1670249). Cells were incubated in a humidified incubator (Heal Force, No. HF90/HF240) at 37 ℃ with an atmosphere of 5% CO_2. For cell passage, cells were digested using 0.25% trypsin–EDTA (Gibco, Cat. 25200056) and passaged every 3 days for further analyses.

STLC was prepared as the 10 mM stock in DMSO and stored at − 20 ℃. For Eg5 inhibition, the GC-2 spd cells were treated with a series of concentrations of STLC for different periods as indicated in each figure and figure legend. For Eg5 knockdown, the GC-2 spd cells were transfected with negative control, FAM, siGAPDH, and the *Eg5*-specific siRNA oligonucleotides using lipofectamine RNAiMAX transfection reagents (Thermo Fisher Scientific, Cat.13778030) according to the manufacturer's instructions, respectively. Cells were then cultured for 24 or 48 h as indicated in figure legends. The efficiency of *Eg5* gene knockdown was validated using PCR analyses and Western blot analyses. The sequences of the siRNAs

were listed as follows: negative control, 5′-UUCUCC GAACGUGUCACGUTT-3′; si*Eg5*-1,5′-CCUUGAUGA AUGCUUACUCUATT-3′; si*Eg5*-2, 5′-AGUUGCUUA ACACGGUUAAAGTT-3′; si*Eg5*-3, 5′-AGCUGAGGU CUACUGAUAUAATT-3′ (*Mus musculus Eg5*, GenBank Accession No. NM_010615.2).

Immunofluorescence and confocal microscopy

For immunofluorescence, the testes were fixed in 10% formaldehyde at room temperature for 12 h and then incubated in 70% ethanol for 1 h, in 85% ethanol for 1 h, in 95% ethanol for 1 h, and in 100% ethanol for 1 h. After being incubated with xylene for 40 min, the testes were incubated with paraffin at 65 ℃ for 1 h and then embedded in paraffin. The 5-μm-thick slides were prepared using an ultramicrotome (Leica No. RM2235) and then incubated in an incubator at 37 ℃ for 12 h. The GC-2 spd cells were seeded on the 12-mm coverslips and cultured in DMEM/high-glucose medium. For fixation, cells were fixed with 4% paraformaldehyde at room temperature for 10 min and then rinsed with PBS for 15 min.

The samples were permeabilized with 0.25% Triton X-100 in PBS at room temperature for 10 min and then rinsed with PBS for 15 min. For antigen blocking, the samples were blocked with 1% bovine serum albumin (BSA)/PBST (0.1% Tween-20 in PBS) at room temperature for 1 h. The samples were incubated with the primary antibodies in 1% BSA/PBST at 37 ℃ for 1 h and then at 4 ℃ overnight. After being rinsed with PBS for 15 min, the samples were incubated with the secondary antibodies in 1% BSA/PBST at room temperature for 2 h in the dark. The samples were rinsed in PBS for 15 min and then stained by the DAPI solution (4,6-diamino-2-phenyl indole, Beyotime, Cat. C1006). The samples were mounted with the anti-fade mounting medium (Beyotime, Cat. P0126). The images were visualized by a Nikon Ti-S2 fluorescence microscope equipped with a Plan-Apochromat 40×/0.75 NA objective and the 405-, 488-, and 561-nm excitation laser. Images were captured by a Nikon DS-Ri2 camera and analyzed using the ImageJ software (NIH).

For immunofluorescence, the primary antibodies used in this study were listed as follows: rabbit anti-β-tubulin monoclonal antibody (Beyotime, Cat. AF1216, 1:250), mouse anti-tubulin monoclonal antibody (Beyotime, Cat. AT819, 1:500), mouse anti-Eg5 monoclonal antibody (Abcam, Cat. ab51976, 1:100), mouse anti-γ-tubulin monoclonal antibody (D-10) (Santa Cruz Biotechnology, Cat. sc-17788, 1:100), mouse anti-PRC1 monoclonal antibody (C-1) (Santa Cruz Biotechnology, Cat. sc-376983, 1:100), rabbit anti-KIF4A polyclonal antibody (Sangon Biotech, Cat. D161832-0025, 1:100). The secondary antibodies were listed as follows: Alexa Fluor 488-conjugated goat anti-rabbit IgG (H + L) (Beyotime, Cat. A0423, 1:500), Alexa Fluor 488-conjugated goat anti-mouse IgG (H + L) (Beyotime, Cat. A0428, 1:500), Alexa Fluor 555-conjugated donkey anti-mouse IgG (H + L) (Beyotime, Cat. A0460, 1:500), Alexa Fluor 555-conjugated donkey anti-rabbit IgG (H + L) (Beyotime, Cat. A0453, 1:500).

Hematoxylin–eosin staining and the Giemsa staining

For HE staining, the slides were incubated in xylene for 40 min, in 100% ethanol for 6 min, in 95% ethanol for 2 min, in 90% ethanol for 2 min, in 80% ethanol for 2 min, and in 70% ethanol for 2 min. After being rinsed in distilled water for 5 min, the slides were stained with Mayer's hematoxylin solution for 6 min at room temperature and then washed with tap water for 5 min. After being incubated with ethanol hydrochloride for 3 s, the samples were washed in tap water for 3 min. The samples were incubated with lithium chloride for 1 min and then were stained with 1% eosin for 5 min. After being rinsed in 95% ethanol for 10 s, the samples were incubated with 100% ethanol for 2 min and in xylene for 5 min. The slides were sealed with neutral gum at room temperature for 2 h.

For the Giemsa staining, cells were fixed with 4% paraformaldehyde for 10 min and then rinsed with distilled water for 5 min. The samples were stained by the Giemsa staining solution supplemented with phosphate buffer (pH 6.8) at room temperature for 15 min. The samples were rinsed with distilled water for 10 min and then sealed with glycerol.

Cell growth curve and cell viability assay

For cell growth curve assay, the GC-2 spd cells were seeded in 24-well plates and incubated with STLC at a final concentration of 1 μM for 6 days. Cells were harvested using 0.25% trypsin/EDTA every 24 h and were counted and recorded using a hemocytometer and a light microscope (Nikon, No. E100).

For cell viability assay, the GC-2 spd cells were seeded in the 12-well plates at approximately 50% confluence for 24 h and then incubated with STLC at a final concentration of 1 μM. Cells were then cultured for 48 and 72 h and then harvested using 0.25% trypsin–EDTA (Gibco). Relative cell viability was measured using the CellTiter 96 aqueous one solution cell proliferation assay (Promega, Cat. G3580) according to the manufacturer's protocols. Luminescence was measured in 96-well flat-bottom polystyrene microplates (Corning, Cat. 3599) at A_{590nm} using a microplate reader (BioTek, No. 180316F).

Colony formation assay

For colony formation assay, approximately 1000 GC-2 spd cells were seeded on each 6-well plate (Corning, Cat. 3516) for 24 h and then incubated with 1 μM STLC in DMEM/high-glucose medium for 2 weeks. After fixing with 1% paraformaldehyde for 10 min, cell colonies were stained with 0.1% crystal violet at room temperature for 15 min. The crystal violet was eluted with 10% acetic acid solution. The eluted solution was measured at A_{590nm} using a microplate reader (BioTek, No. 180316F).

Scratch wound healing assay

The GC-2 spd cells were seeded in the 24-well plates at 80–90% density and then cultured for 24 h to reach 100% density. Three parallel straight lines were generated across the monolayer cells and a fresh medium was used to slowly wash away the detached cells. The GC-2 spd cells were incubated with 0.5, 1, 5, and 25 μM STLC, respectively. After being cultured for 12, 18, and 24 h, the gap of monolayer cells was recorded and analyzed using an inverted microscope (Jiangnan, No.XD-202).

Flow cytometry

For cell cycle analysis, the GC-2 spd cells were dissociated by 0.25% trypsin–EDTA at 37 ℃ for 1 min and then centrifuged at 1000 rpm/min for 5 min. After being rinsed in PBS for 2 min, cells were fixed in 70% cold ethanol at 4 ℃ for 12 h. Cells were incubated with the propidium iodide staining solution (0.1% Triton X-100/PBS, 20 μg/ml RNase A, and 50 μg/ml propidium iodide; Beyotime, Cat. C1052) at 37 ℃ for 1 h. The samples were analyzed at the excitation wavelength of 488 nm using a flow cytometer (BD, FACSCanto™ II). Cell DNA content and light scattering analyses were performed using the ModFit LT32 software (Verity Software House).

Western blotting

The GC-2 spd cells were lysed in 3% SDS lysis buffer on the ice and incubated on ice for 10 min. The samples were incubated at 100 ℃ for 10 min. The proteins were separated on 5% and 10% polyacrylamide gels and transferred onto PVDF membranes (GE, Cat. 10600023). Membranes were washed three times with PBST and then blocked with 3% BSA/PBST for 1 h. The membranes were incubated with diluted primary antibodies in 3% BSA/PBST at 4 ℃ overnight. The membranes were washed by PBST for 15 min and incubated with the diluted secondary antibodies in 3% BSA/PBST at room temperature for 2 h and then washed with PBST for 15 min. Immunoblots were imaged on a ChemiDoc™ Touch Imaging System (Bio-Rad). The quantifications were measured and analyzed by the ImageJ software (NIH). The antibodies used in western blot were listed as follows: rabbit monoclonal anti-Eg5 antibody (Abcam, Cat. ab254298, 1:1000), HRP-conjugated goat anti-rabbit IgG (Sangon Biotech, Cat. D110058-0100, 1:1000), and anti-GAPDH-HRP antibody (GNI, Cat. GNI4310-GH-S, 1:5000).

Statistical analysis

All experiments were replicated independently at least three times or more on separate days. All sample sizes were indicated in each figure legend. No statistical methods were used to predetermine the sample size. The investigators were not blinded to allocation during experiments and outcome assessment. The stages of seminiferous tubules were clarified according to the standard guidelines (Leblond and Clermont 1952a, b; Russell et al. 1990). Immunofluorescence images were analyzed by the Image J software (NIH) to compare fluorescence intensities. For all bar graphs, mean ± SEM were shown. Statistical significances between groups were determined by the unpaired two-tailed student's *t* test and then computed by the GraphPad Prism 6.0 software (GraphPad). *P* values less than 0.05 were considered significant. ns, $P > 0.05$; *, $P < 0.05$; **, $P < 0.01$; ***, $P < 0.001$; ****, $P < 0.0001$.

Results

Kinesin-5 Eg5 plays an essential role in mouse spermatocytes in vivo and in vitro

Firstly, we performed the immunofluorescence assay to study the localization of Eg5 proteins in spermatogenic cells. We found that Eg5 proteins were expressed in the spermatocytes and mainly enriched at spindle microtubules in dividing spermatocytes of 3-week-old male mouse testes (Fig. 1a). A portion of Eg5 proteins accumulated at the spindle proximal to the spindle poles and co-localized with microtubules (Fig. 1a).

To further investigate the functions of Eg5 proteins in spermatogenesis, we constructed a mouse model through intraperitoneal injection of Eg5-specific inhibitor STLC at a final concentration of 1 μM STLC every 2 days for 2 weeks (Fig. 1b–e). We observed an increased number of metaphase-arrested spermatocytes in the STLC-treated testes (Fig. 1b, c). In seminiferous tubules, the distribution of spermatogenic cells was regular in control while spermatogenic cells were disorderly arranged in the STLC group (Fig. S1a). Furthermore, the immunofluorescence results revealed that the spermatocytes with monopolar spindles significantly increased after Eg5 inhibition (Fig.1d–f).

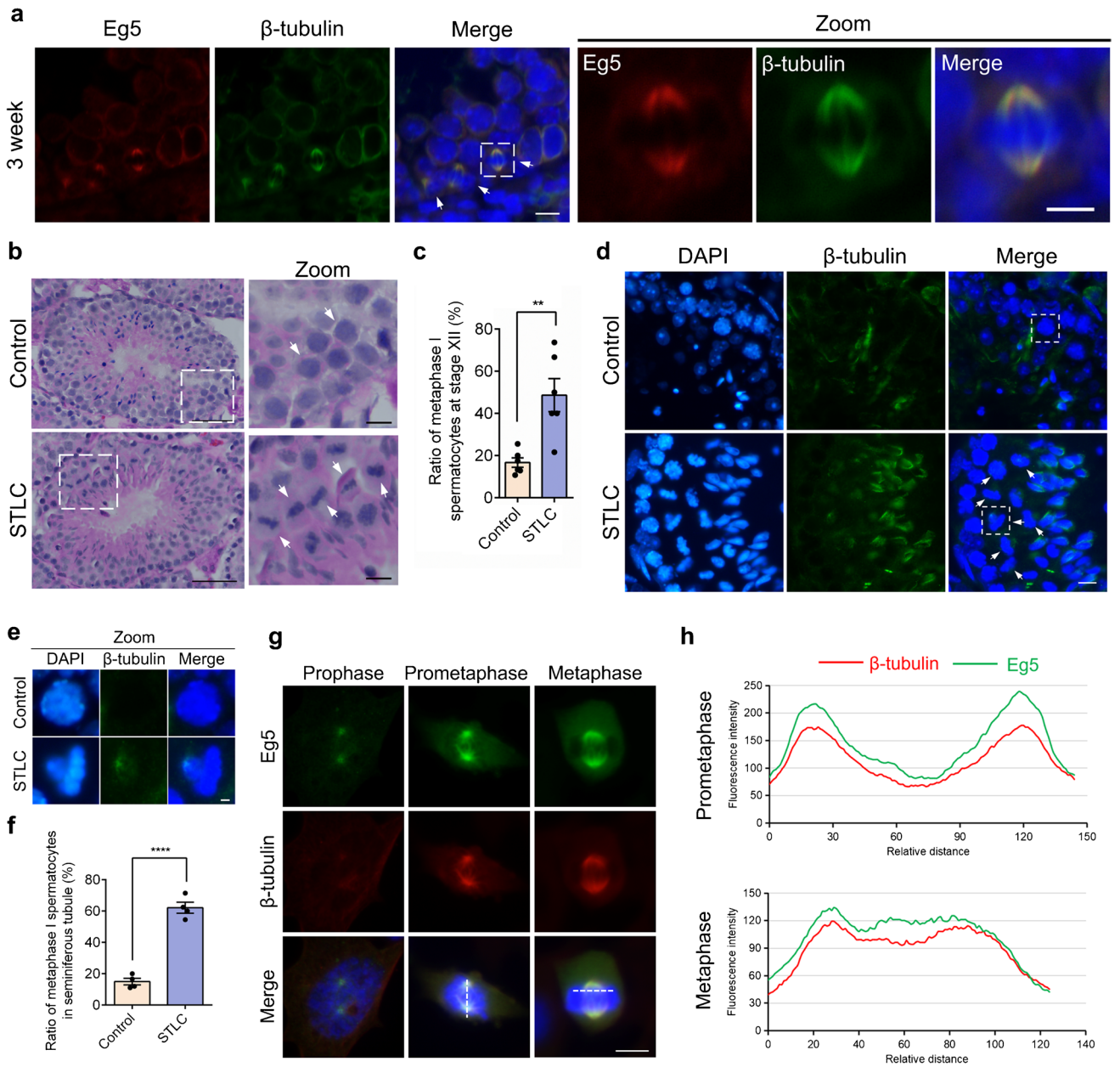

Fig. 1 Eg5 inhibition resulted in metaphase arrest of spermatocytes. **a** Immunofluorescence images of the seminiferous tubule of the untreated 3-week-old male mouse. Eg5 (red), β-tubulin (green), and DAPI (blue). White arrows indicate the spermatocytes during metaphase. Scale bar, 10 μm and 5 μm (Zoom). **b** HE staining of seminiferous tubules (stage X) in the control and 1 μM STLC groups. Eg5 inhibition led to metaphase-arrested spermatocytes. Scale bar, 50 μm. The magnified images from dashed boxes were shown. White arrows indicate the spermatocytes. Scale bar, 10 μm. **c** Ratio of metaphase I spermatocytes at stage XII in the control and STLC groups were shown. Control, 16.6 ± 2.25%; STLC, 48.66 ± 7.82%. Group = 6. **d–e** Immunofluorescence images of seminiferous tubules (stage X) in the control and 1 μM STLC groups. Eg5 inhibition contributed to the metaphase-arrested spermatocytes and monoastral spindles. β-tubulin (green) and DAPI (blue). White arrows indicate metaphase-arrested spermatocytes. Scale bar, 10 μm and 2 μm (Zoom). **f** Ratio of metaphase I spermatocytes in seminiferous tubules in the control and STLC groups were shown. Control, 14.94 ± 2.08%; STLC, 62.12 ± 3.52%. Group = 4. **g** Representative immunofluorescence images of Eg5 proteins in the GC-2 spd cells. Eg5 proteins mainly located at the centrosomes and the spindle microtubules from prophase to metaphase. Eg5 (green), β-tubulin (red), and DAPI (blue). Scale bar, 10 μm. **h** The co-localization patterns of Eg5 and β-tubulin were analyzed by the ImageJ software. Eg5 (green) and β-tubulin (red). The X axis indicates the relative distance and the Y axis indicates fluorescence intensities. Student's *t* test. Error bars, mean ± SEM. **, $P < 0.01$; ****, $P < 0.0001$

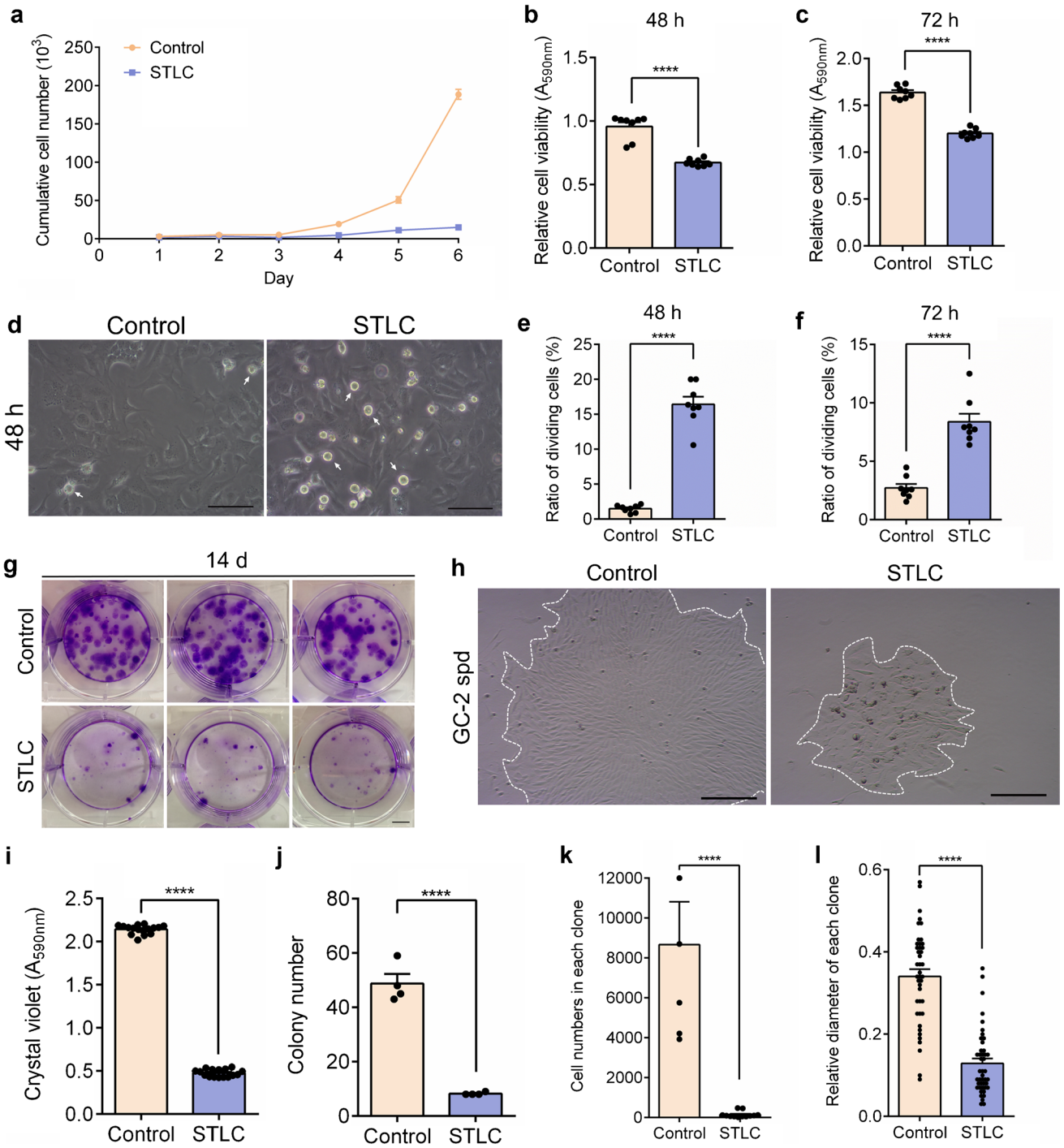

Together, these results show that Eg5 inhibition leads to a significant increase of metaphase-arrested spermatocytes and monopolar spindles, indicating Eg5 proteins are critical for the meiosis of spermatocytes in vivo.

In order to study the functions of Eg5 in cell division of spermatocytes, we used the GC-2 spd cell line as our model cell line which was established by stable transfection of the SV40 large T antigen gene and the *p53* gene (Hofmann et al. 1994, 1995; Chimento et al. 2012). The GC-2 spd cell is an immortalized mouse pachytene spermatocyte-derived cell line, which is a useful tool for the studies of spermatocytes in vitro (Chen et al. 2012; Chimento et al. 2012; Zhang et al. 2018; She et al. 2020). We performed the immunofluorescence assay to explore the localization of Eg5 proteins in cultured GC-2 spd cells. Eg5 proteins were distributed in the cytoplasm at interphase and then co-localized with spindle microtubules at prophase (Fig. 1g). In prometaphase and metaphase, Eg5 proteins mainly accumulated at the spindle

◂**Fig. 2** Eg5 inhibition led to the significant decreases in cell numbers, cell viability, and cell colonies of the GC-2 spd cells. **a** The growth curve analysis of the GC-2 spd cells in the control and 1 μM STLC groups. The X axis indicates the time of treatment (day), and the Y axis indicates the cumulative cell number ($\times 10^3$). **b–c** Relative cell viability (A_{590nm}) of the control and 1 μM STLC groups after Eg5 inhibition for 48 and 72 h, respectively (48 h, 0.96 ± 0.03 in control and 0.67 ± 0.01 in STLC; 72 h, 1.64 ± 0.02 in control and 1.20 ± 0.02 in STLC). $n = 8$ per group. **d** Representative images of the GC-2 spd cells incubated with 1 μM STLC for 48 and 72 h, respectively. White arrows indicate the dividing cells. Scale bar, 50 μm. **e** Ratio of dividing cells in the control and 1 μM STLC groups (48 h). Control, 1.50 ± 1.08%; STLC, 16.43 ± 1.07%. Control, $n = 2690$. STLC, $n = 1660$. Group = 8. **f** Ratio of dividing cells in the control and 1 μM STLC groups (72 h). Control, 2.72 ± 0.34%; STLC, 8.38 ± 0.70%. Control, $n = 699$. STLC, $n = 1435$. Group = 8. **g** Colony formation analysis of the control and 1 μM STLC groups after treatment for 14 days. Scale bar, 3.1 mm. **h** Representative images of the colony in the control and 1 μM STLC groups. Scale bar, 50 μm. **i** Crystal violet (A_{590nm}) was measured in the control and 1 μM STLC groups (control, 2.14 ± 0.01; STLC, 0.48 ± 0.01). $n = 16$ per group. **j** The colony numbers were measured in the control and 1 μM STLC groups (control, 48.75 ± 3.57; STLC, 8.25 ± 0.25). $n = 4$ per group. **k** Cell numbers in each colony were measured in the control and 1 μM STLC groups (control, 8667 ± 2146; STLC, 144.1 ± 44.62). $n = 6, 12$. **l** The diameters of each colony were measured in the control and 1 μM STLC groups (control, 0.34 ± 0.02; STLC, 0.13 ± 0.01). $n = 42, 44$. Student's t test. Error bars, mean ± SEM. ****, $P < 0.0001$

microtubules (Fig. 1h). We revealed the co-localization between Eg5 and β-tubulin on spindle microtubules from prophase to metaphase (Fig. 1h). Eg5 proteins remained at the spindle poles at anaphase A and gradually translocated to the central spindle at anaphase B (Fig. S1b). During telophase, Eg5 proteins accumulated in the midbody and showed co-localization with β-tubulin (Fig.S1b, c). Taken together, these results elucidate expression patterns of Eg5 proteins in cell division of spermatocytes both in vivo and in vitro.

Eg5 is crucial for the proliferation, colony formation, and migration of the GC-2 spd cells

The cell growth curve experiment showed that cell proliferation of the GC-2 spd cells was significantly suppressed after Eg5 inhibition in the 1 μM STLC group compared with the control group. In control, the GC-2 spd cells proliferate faster after 4 days and reached the exponential growth period. However, the GC-2 spd cells proliferate slowly in the STLC group (Fig. 2a). Next, we selected STLC with a series of concentration gradients, including 0.1, 0.25, 0.5, and 1 μM, for the inhibition of Eg5 proteins (Fig. S2a). We observed that after incubation with STLC for 12 h, the ratios of dividing cells increased to 3.09% in the 0.1 μM group, significantly increased to 3.35% in the 0.25 μM group, 6.39% in the 0.5 μM group, and 21.25% in the 1 μM group, compared with 1.87% in the control group (Fig. S2b). These results indicate that Eg5 is required for cell proliferation of the GC-2 spd cells.

We then used 1 μM STLC to inhibit Eg5 for 48 and 72 h to observe cell morphology. The cell viability assay demonstrated that the relative cell viability was significantly decreased by 30.21% at 48 h and 26.83% at 72 h (Fig.2b, c). Eg5 inhibition resulted in a significant increase of metaphase-arrested cells among the GC-2 spd cells (Fig.2d–f). These results suggest that Eg5 inhibition leads to the decrease of cell viability and cell cycle arrest of the GC-2 spd cells.

Furthermore, we performed colony formation assays to investigate the long-term Eg5 inhibition effects on the GC-2 spd cells (Fig.2g–1). In the STLC group, we found the number of cell colonies was markedly reduced and the sizes of cell colonies were decreased in parallel with control (Fig.2g, h). Compared with the control, the crystal violet (A_{590nm}) was significantly reduced by 77.57% (Fig. 2i) and the number of cell colonies was dramatically decreased by 83.08% (Fig. 2j). Moreover, cell numbers in each clone were decreased by 98.34% (Fig. 2k), and the diameter of each clone was markedly decreased by 61.76% (Fig. 2l). Consistent with the cell viability assays, these results indicate that Eg5 inhibition severely suppresses the proliferation capacity and the colony formation of the GC-2 spd cells.

We next performed the scratch wound healing assays to measure the migration of the GC-2 spd cells after treatment with a series of STLC for 12, 18, and 24 h. Eg5 inhibition led to longer wound distances and slower wound healing rates. The wound distance was significantly increased in different concentrations of STLC groups compared with the control group (Fig.S2d–f). Particularly, in 24 h, the wound distance showed an increase of direct proportion with incremental concentrations of STLC (Fig. S2d). Compared with the low-dose groups (1 μM STLC), the high-dose groups (25 μM STLC) were increased by 7.89% in 12 h, 13.11% in 18 h, and 40.00% in 24 h (Fig. S2d–f). The cell viability of the GC-2 spd cells was markedly decreased after Eg5 inhibition for 48 h (Fig. S2g). Together, Eg5 proteins are responsible for cell proliferation, colony formation, and cell migration of the GC-2 spd cells.

Eg5 inhibition leads to metaphase arrest, abnormal nuclei, and spindle disorganization in spermatocytes

We used flow cytometry to study the cell cycle of the GC-2 spd cells, including the G_0/G_1 phase, the S phase, and the G_2/M phase (Fig. 3). The GC-2 spd cells were incubated by 1 μM STLC for 48 h. In the 48-h STLC group, the ratio of the G_0/G_1 phase cells significantly reduced to 22.97% compared with 44.94% in control (Fig. 3a, b), the ratio of the S phase cells markedly decreased to 34.53% compared with 42.71% in control (Fig. 3c), and the ratio of the G_2/M phase cells dramatically increased to 42.50% compared with

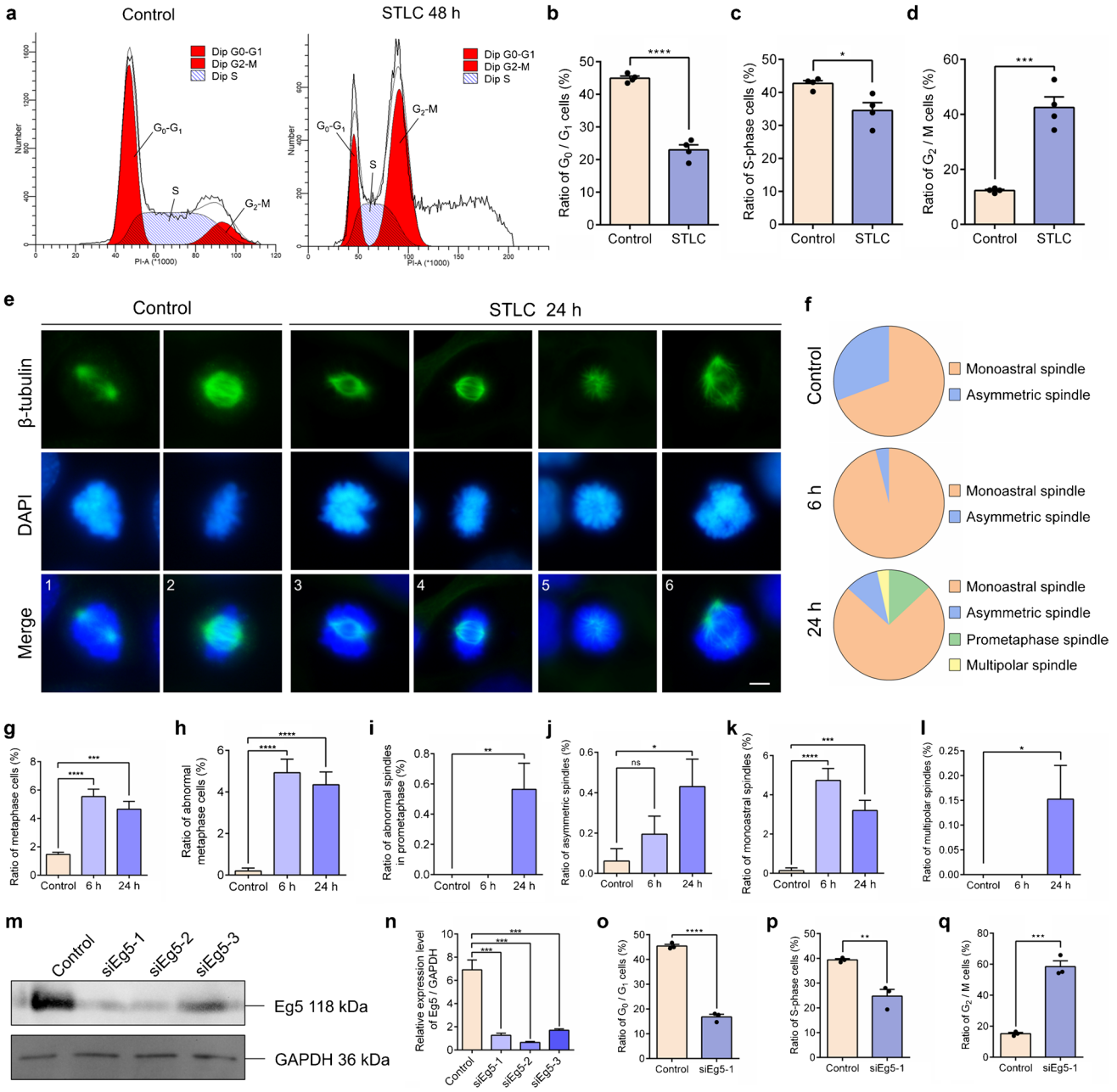

Fig. 3 Eg5 inhibition caused metaphase arrest and spindle disorganization of the GC-2 spd cells. **a** Flow cytometry analysis of the GC-2 spd cells in the control and 1 μM STLC groups (48 h). $n = 30{,}000$ were analyzed in each group. Group = 4. **b–d** The ratios of the G_0/G_1 cells, the S-phase cells, and the G_2/M cells. G_0/G_1, 44.94 ± 0.65% in control and 22.97 ± 1.54% in STLC; S-phase, 42.71 ± 0.84% in control and 34.53 ± 2.35% in STLC; G_2/M, 12.35 ± 0.38% in control and 42.50 ± 3.88% in STLC. $n = 4$ per group. **e** The control cells in prometaphase (1) and metaphase (2) were shown. Eg5 inhibition by 1 μM STLC for 24 h resulted in spindle disorganization in metaphase, including the abnormal spindle in metaphase (3), the asymmetric spindle (4), the monoastral spindle (5), and the multipolar spindle (6). β-tubulin (green) and DAPI (blue). Scale bar, 5 μm. **f** The ratios of metaphase cells with monoastral spindle or asymmetric spindle in the control, 6 h STLC and 24 h STLC groups. **g** The ratios of metaphase cells in the control, 6 h STLC and 24 h STLC groups. **h** The ratios of abnormal metaphase cells in the control, 6 h STLC and 24 h STLC groups. **i** The ratios of abnormal spindles in prometaphase in the control, 6 h STLC and 24 h STLC groups. **j** The ratios of asymmetric spindles in the control, 6 h STLC and 24 h STLC groups. **k** The ratios of monoastral spindles in the control, 6 h STLC and 24 h STLC groups. **l** The ratios of multipolar spindles in the control, 6 h STLC and 24 h STLC groups. $n = 6$ per group. **m** Western blotting analysis of the GC-2 spd cells transfected with the siRNAs for 30 h. Eg5 proteins were significantly attenuated in *Eg5*-specific siRNA transfected cells. **n** Relative expression levels of Eg5/GAPDH in the control, siEg5-1, siEg5-2 and siEg5-3 groups were shown (control, 6.91 ± 0.85; SiEg5-1, 1.27 ± 0.18; siEg5-2, 0.66 ± 0.08; siEg5-3, 1.70 ± 0.12). $n = 4$ per group. **o–q** Flow cytometry analyses of the GC-2 spd cells in the control and siEg5-1 groups (32 h). The ratios of the G_0/G_1 phase cells, the S-phase cells and the G_2/M phase cells were shown. Group = 3. $n = 30{,}000$ were analyzed in each group. Student's t test. Error bars, mean ± SEM. ns, $P > 0.05$; *, $P < 0.05$; **, $P < 0.01$; ***, $P < 0.001$; ****, $P < 0.0001$

12.35% in control (Fig. 3d). These results reveal that Eg5 inhibition leads to the reduction of the G_0/G_1 phase and the increase of the G_2/M phase cells, indicating Eg5 suppression contributes to cell cycle arrest at the G_2/M phase.

Next, we performed the Giemsa staining assay and the immunofluorescence assay to analyze the nuclear morphology of the GC-2 spd cells after Eg5 inhibition. The GC-2 spd cells were incubated with 0.1, 0.5, 1, 5, and 10 μM STLC for 24 h, respectively (Fig. S3). The ratios of metaphase cells increased to 3.35–17.59% compared with 3.33% in control, indicating Eg5 inhibition led to gradually increased metaphase-arrested cells with the increased concentrations of STLC (Fig. S3c). There were different abnormalities in interphase cells, including heteromorphic nuclear cells, small nuclear cells, binuclear cells, and multinucleate cells with two or more nuclei (Fig. S3b, d). The ratios of interphase cells with the irregular nucleus increased to 6.31–15.88% compared with 4.43% in control (Fig. S3e). The ratios of heteromorphic nuclear cells increased to 2.49–8.40% compared with 1.96% in control (Fig. S3f). The ratios of small nuclear cells increased to 0.53–3.12% compared with 0.18% in control (Fig. S3g). These results indicate that Eg5 inhibition leads to various deformities in the nucleus. In addition, compared with 1.61% in control, the ratio of total apoptotic cells was significantly increased to 4.22% in the 10 μM STLC group (Fig. S3h). Together, Eg5 inhibition contributes to the increased number of metaphase-arrested cells and diverse nuclear abnormalities in interphase cells.

Then, we used the immunofluorescence assay to study spindle organization and chromosome alignment in the GC-2 spd cells after Eg5 inhibition (Fig. 3e–f). These cells were cultured with 1 μM STLC for 6 and 24 h, respectively. The ratios of metaphase cells significantly increased to 4.65–5.54% compared with 1.47% in control (Fig. 3g), indicating Eg5 inhibition led to metaphase arrest of GC-2 cells. In metaphase cells, the ratios of abnormal cells dramatically increased to 4.35–4.93% compared with 0.20% in control (Fig. 3h). The ratios of metaphase cells with monoastral spindle or asymmetric spindle increased in the 24-h-treated group compared with the 6-h-treated group (Fig. 3i). After incubating with STLC for 24 h, we found four kinds of spindle deformities during prometaphase and metaphase, including the abnormal spindle in prometaphase, the asymmetric spindle, the monoastral spindle, and the multipolar spindle (Fig. 3i–1). The chromosome misalignment was related to impaired spindle microtubules, causing deformities of both monopolar spindles and bipolar spindles. The monoastral spindle was the major type among abnormal metaphase cells, and the ratios of monoastral spindles significantly increased to 3.20–4.73% compared with 0.14% in control (Fig. 3k). The ratios of asymmetric spindles increased to 0.19–0.43% compared with 0.06% in control (Fig. 3j). In the 24-h-treated group, the ratio of abnormal spindles in prometaphase increased to 0.56% compared with 0.00% in control (Fig. 3i), and the ratio of multipolar spindles significantly increased to 0.15% compared with 0.00% in control (Fig. 3l). In conclusion, Eg5 inhibition leads to the formation of monopolar spindles, the malformation of bipolar spindles, and the misalignment of chromosomes.

Eg5 knockdown results in spindle disorganization and chromosome misalignment in dividing spermatocytes

To further study functions and mechanisms of Eg5 depletion in the GC-2 spd cells, we used the siRNAs to transfect these cells (Fig. 3m, n; Fig. 4; Fig. S4, S5). Western blotting analyses revealed siRNA transfection significantly reduced the expression level of Eg5 proteins and the relative expression levels of Eg5/GAPDH decreased by 75.40–90.45%, indicating *Eg5* was effectively knockdown by *Eg5*-specific siRNA (Fig. 3m, n). Consistent with these results, the fluorescent intensities of Eg5 proteins dramatically reduced after siRNA transfection (Fig. S4a). After Eg5 depletion for 24 h, the ratios of dividing cells significantly increased to 10.84–29.89% compared with 5.15% in control (Fig. S4b, c). Together, these results suggest that siRNA transfection efficiently reduces the expression of Eg5 proteins.

Flow cytometry analyses indicated cell cycle alteration of the GC-2 spd cells after Eg5-specific siRNA transfection for 32 h (Fig. 3o–q). The ratio of G_0/G_1 phase cells markedly decreased to 16.83% compared with 45.44% in control (Fig. 3o), the ratio of S phase cells dramatically decreased to 24.76% compared with 39.38% in control (Fig. 3p), and the ratio of G_2/M phase cells significantly increased to 58.41% compared with 15.18% in control (Fig. 3q). Taken together, Eg5 depletion contributes to the increase of dividing cells and the cell arrest at the G_2/M phase.

We performed the immunofluorescence assay to study the spindle organization of the GC-2 spd cells during metaphase after Eg5 knockdown for 24 h (Fig. 4; Fig. S5a). The ratios of metaphase cells dramatically increased to 4.93–16.06% compared with 2.36% in control (Fig. 4c), indicating Eg5 knockdown contributed to metaphase arrest of GC-2 spd cells. Consistent with the STLC-mediated Eg5 inhibition, the results showed four abnormal spindles, including abnormal spindles in prometaphase, asymmetric spindles, monoastral spindles, and multipolar spindles (Fig. 4a; Fig. S5a). Compared with 0.14% in control, the ratios of abnormal metaphase cells significantly increased to 4.46–15.70% (Fig. 4d). The monoastral spindle was the major type of the siRNA-transfected groups (Fig. 4b), and the ratios of monoastral spindles markedly increased to 3.29–15.70% compared with 0.00% in control (Fig. 4e). Taken together, siRNA-mediated *Eg5*

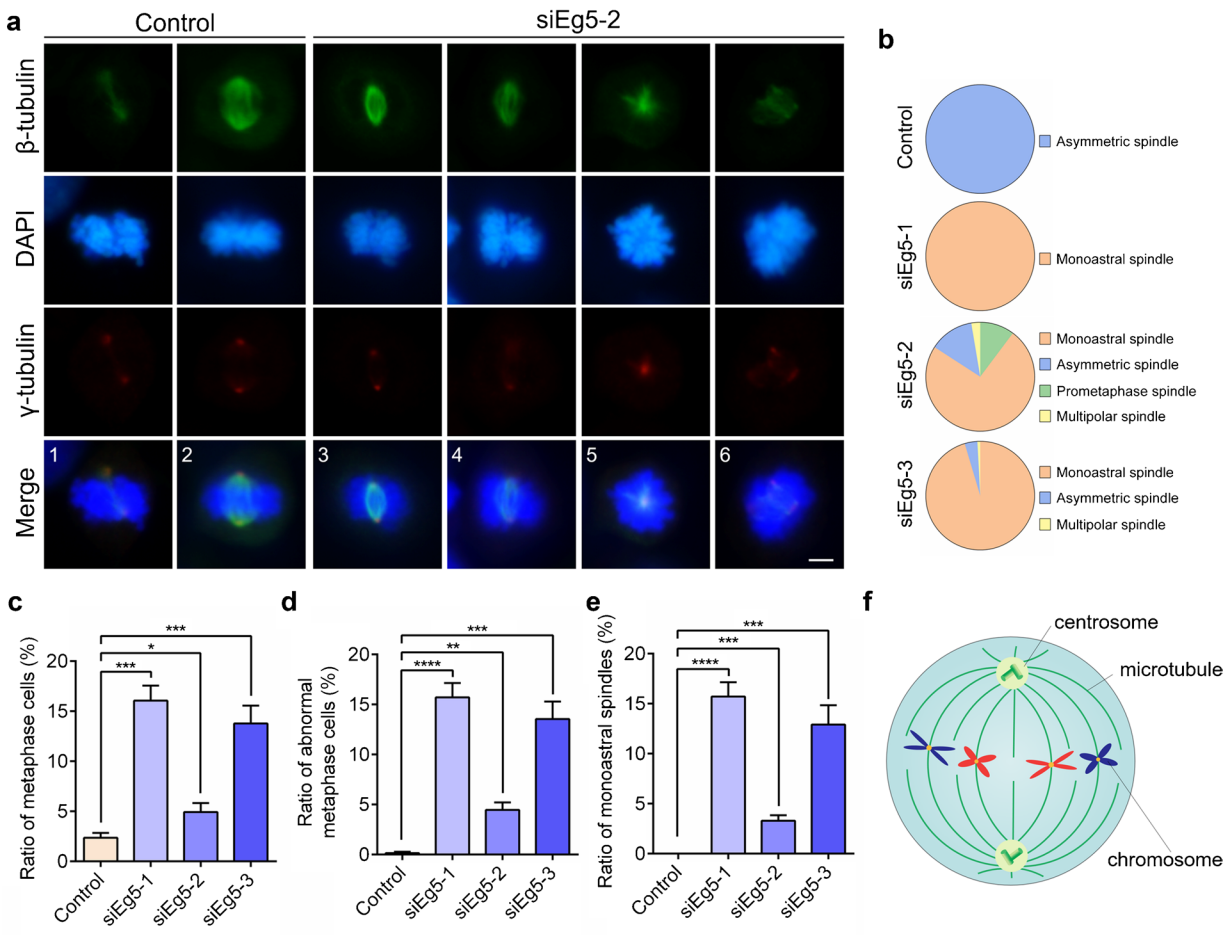
a
Control
siEg5-2
β-tubulin
DAPI
γ-tubulin
Merge
1
2
3
4
5
6
b
Control
siEg5-1
siEg5-2
siEg5-3
Asymmetric spindle
Monoastral spindle
Prometaphase spindle
Multipolar spindle
c
Ratio of metaphase cells (%)
d
Ratio of abnormal metaphase cells (%)
e
Ratio of monoastral spindles (%)
Control
siEg5-1
siEg5-2
siEg5-3
f
centrosome
microtubule
chromosome

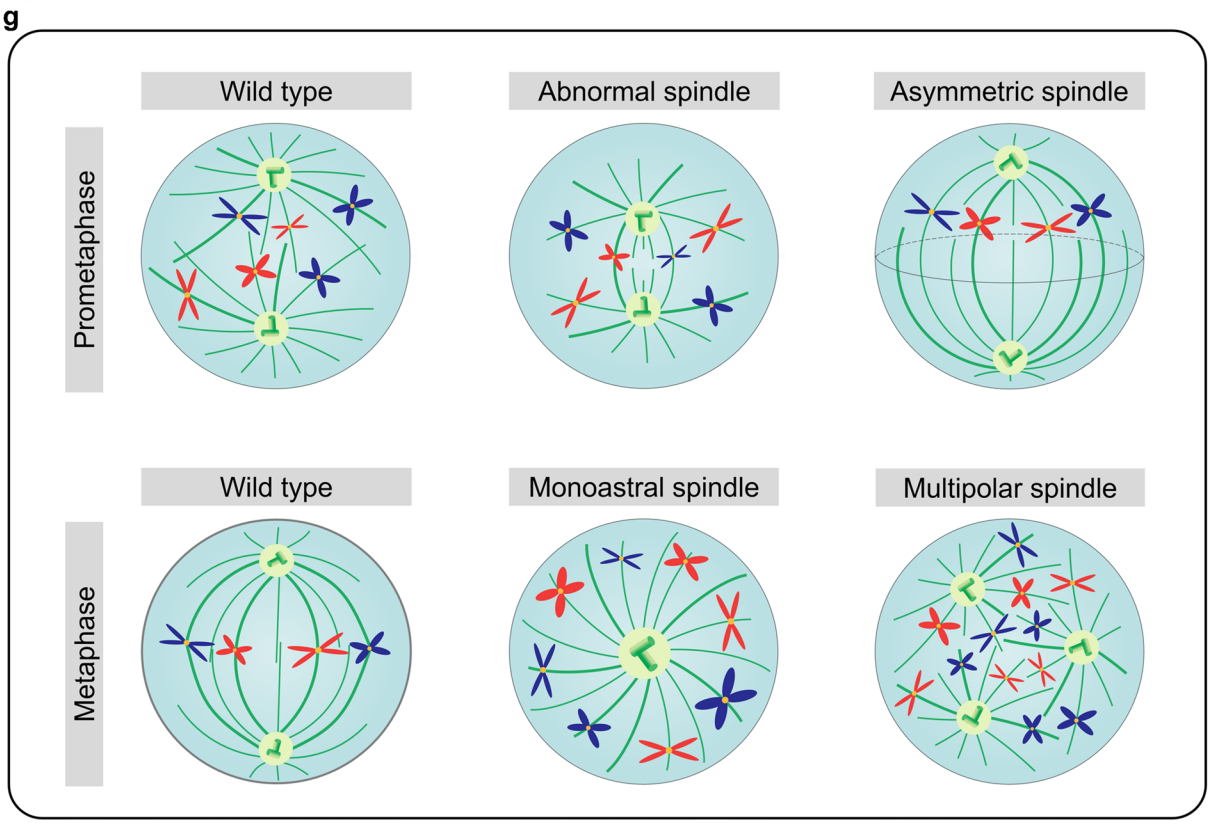
g
Prometaphase
Metaphase
Wild type
Abnormal spindle
Asymmetric spindle
Wild type
Monoastral spindle
Multipolar spindle

◂**Fig. 4** *Eg5* depletion led to metaphase arrest and spindle disorganization of the GC-2 spd cells. **a** Immunofluorescence images of the GC-2 spd cells in the control and siEg5-2 groups. The control cells were shown during prometaphase (1) and metaphase (2). *Eg5* knockdown by siRNA transfection for 24 h led to spindle abnormalities in metaphase, including the abnormal spindle in prometaphase (3), the asymmetric spindle (4), the monoastral spindle (5), and the multipolar spindle (6). β-tubulin (green), DAPI (blue) and γ-tubulin (red). Scale bar, 5 μm. **b** The ratios of abnormal metaphase cells in the control, siEg5-1, siEg5-2, and siEg5-3 groups (control, 0.14%; siEg5-1, 15.70%; siEg5-2, 4.46%; siEg5-3, 13.54%). $n=4$ per group. **c** The ratios of metaphase cells in the control, siEg5-1, SiEg5-2, and SiEg5-3 groups were shown (control, 2.36 ± 0.47%; SiEg5-1, 16.06 ± 1.50%; SiEg5-2, 4.93 ± 0.90%; SiEg5-3, 13.78 ± 1.79%). $n=4$ per group. **d** The ratios of abnormal metaphase cells in the control, SiEg5-1, SiEg5-2 and SiEg5-3 groups were shown (control, 0.14 ± 0.14%; siEg5-1, 15.70 ± 1.44%; siEg5-2, 4.46 ± 0.75%; siEg5-3, 13.54 ± 1.76%). $n=4$ per group. **e** The ratios of monoastral spindles in the control, siEg5-1, siEg5-2, and siEg5-3 groups were shown (control, 0.00 ± 0.00%; siEg5-1, 15.70 ± 1.44%; siEg5-2, 3.29 ± 0.54%; siEg5-3, 12.92 ± 1.93%). $n=4$ per group. Student's *t*-test. Error bars, mean ± SEM. *, $P<0.05$; **, $P<0.01$; ***, $P<0.001$; ****, $P<0.0001$. **f** Representative model of the GC-2 spd cell in metaphase. The centrosomes, microtubules, and chromosomes were shown. **g** Graphical model of Eg5's functions in the GC-2 spd cells during prometaphase and metaphase. In wild-type cells, two centrosomes were nearly located with radial microtubules at prometaphase, and the chromosomes were neatly arranged on the spindle equator at metaphase. After Eg5 inhibition or knockdown, four different types of spindle disorganization were shown. In the abnormal spindle during prometaphase, two centrosomes were proximally positioned with connected microtubules. In the asymmetric spindle, the spindle microtubules showed asymmetric morphology. In the monoastral spindle, the centrosome was surrounded by chromosomes. In the multipolar spindle, the chromosomes were misaligned around three centrosomes

knockdown results in spindle disorganization and defects in spindle pole separation in cultured spermatocytes (Fig. 5g).

The Giemsa staining results illustrated that the nuclear morphology of the GC-2 spd cells was disrupted during interphase after *Eg5* knockdown for 24 h (Fig. S5b–g). Consistent with the STLC-mediated Eg5 inhibition, we observed three kinds of deformities including heteromorphic nuclear cells, small nuclear cells, and multinuclear cells with two or more nuclei (Fig. S5b, c). The ratios of interphase cells with the irregular nucleus increased to 15.04–28.83% compared with 10.48% in control (Fig. S5d). The ratios of heteromorphic nuclear cells increased to 5.84–13.63% compared with 5.09% in control (Fig. S5e). The ratios of small nuclear cells increased to 4.99–15.11% compared with 3.98% in control (Fig. S5f). The ratios of multinucleate cells significantly increased to 4.37–7.35% compared with 1.42% in control (Fig. S5g). In conclusion, siRNA-mediated *Eg5* knockdown disrupts bipolar spindle formation, spindle organization, and chromosome alignment in the GC-2 spd cells (Fig. 4g).

Eg5 regulates centrosome separation and spindle assembly in the GC-2 spd cells

To further investigate the mechanisms of Eg5 in spindle assembly, we incubated the GC-2 spd cells with STLC for 24 h and stained the centrosomes using the immunofluorescence of anti-γ-tubulin antibody (Fig. 5, 6). We observed that spindle microtubules were disorganized and the relative distances of centrosomes markedly decreased by 38.86% in prometaphase (Fig. 5b). Moreover, we found that the distance of centrosomes in metaphase significantly decreased by 91.20% in metaphase (Fig. 5d). The results showed that the separation of centrosomes was blocked and the distance of two spindle poles was reduced after Eg5 inhibition. In most metaphase-arrested GC-2 spd cells, the centrosomes were clustered together to form a single spindle pole and finally resulted in the formation of the monopolar spindle (Fig. 5c). In addition, 0.15% GC-2 spd cells presented multipolar spindles after Eg5 inhibition (Fig. 5c). These results indicate Eg5 inhibition leads to the defects in the separation of the centrosomes during prometaphase and metaphase.

To study the long-term effects of Eg5 inhibition on the GC-2 spd cells, we treated the cells with 0.1, 0.5, and 1 μM STLC for 5 days and examined the number of centrosomes and microtubule using immunofluorescence (Fig. 6). In the control group, 70.74% of the GC-2 spd cells contain 2 centrioles located on the side of the nucleus (Fig. 6a, c). However, in the experimental groups, we found that more than two centrioles were scattered around the nucleus (Fig. 6a, b). As concentrations of STLC increased, the number of centrioles gradually increased in the interphase cells (Fig. 6b). Taken together, the long-term of Eg5 inhibition leads to increasing numbers of centrioles, which is a result of cell cycle arrest.

In addition, we also found that Eg5 inhibition slightly disrupted the spindle organization in the midzone (Fig. S6a–d). The distribution of the marker proteins, including PRC1 and KIF4A, was slightly influenced after Eg5 inhibition (Fig. S6a, c). Meanwhile, the fluorescence intensities of PRC1 and KIF4A were weaker compared with the control (Fig. S6b, d). In the GC-2 spd cells, the midbodies were disrupted after Eg5 inhibition (Fig. S6e–h). The localization of KIF4A and PRC1 was attenuated in the midbodies in the STLC group (Fig. S6e, g). These results indicate that Eg5 also plays a minor role in the assembly of the central spindle and the midbody during cytokinesis.

The short-term inhibition of Eg5 slightly influences the separation of centrosomes during metaphase

We used the immunofluorescence assays to study how Eg5 influences centrosome separation and spindle formation in GC-2 spd cells after the short-term inhibition of Eg5 (Fig. 7;

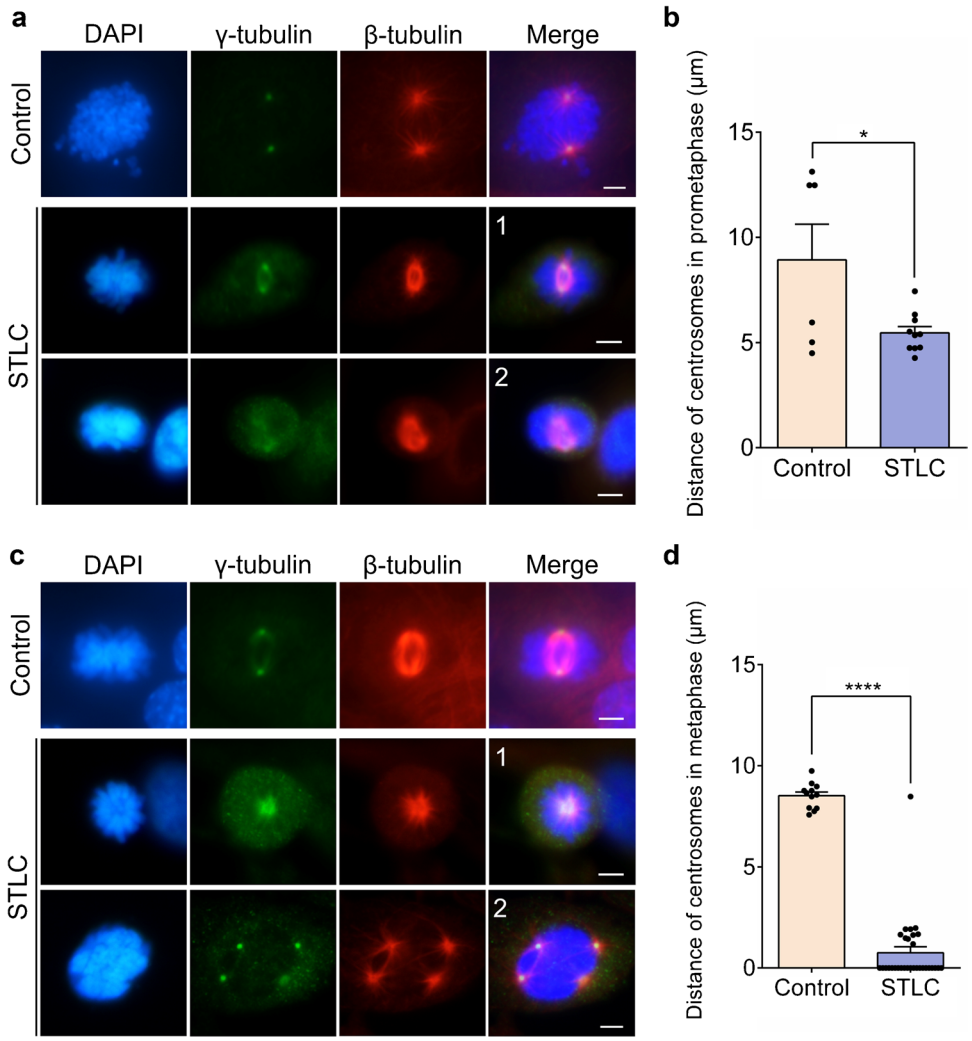

Fig. 5 Eg5 inhibition resulted in abnormal distribution of centrosomes during prometaphase and metaphase. **a** Representative immunofluorescence images of prometaphase cells. Abnormalities in centrosomes, including the abnormal spindle in prometaphase (1) and the asymmetric spindle (2), were shown. The GC-2 spd cells were treated with 1 μM STLC for 24 h. β-tubulin (red), γ-tubulin (green), and DAPI (blue). Scale bar, 5 μm. **b** Distances of two centrosomes in prometaphase were shown (control, 8.93 ± 1.70 μm; STLC, 5.46 ± 0.30 μm). $n = 6$, 10. **c** Representative immunofluorescence images of metaphase cells. The abnormalities in centrosomes, including the monoastral spindle (1) and the multipolar spindle (2), were shown. The GC-2 spd cells were cultured with 1 μM STLC for 24 h. β-tubulin (red), γ-tubulin (green), and DAPI (blue). Scale bar, 5 μm. **d** Distances of centrosomes in metaphase were shown (control, 8.52 ± 0.18 μm; STLC, 0.75 ± 0.29 μm). $n = 12$, 31. Student's *t* test. Error bars, mean ± SEM. *, $P < 0.05$; ****, $P < 0.0001$

Fig. S7). The GC-2 spd cells were incubated with 0.1, 1, and 5 μM STLC for 5 min, 30 min, 1 h, and 5 h, respectively. We observed that the distance of spindle poles was slightly reduced after Eg5 inhibition, suggesting that centrosome separation was suppressed after short-term inhibition of Eg5 (Fig. 7a).

In addition, the ratios of cells in prometaphase and metaphase increased to 1.41–1.77% in the 5 min group compared with 1.10% in control (Fig. 7e), 1.18–1.83% in the 30-min group compared with 0.73% in control (Fig. 7g), 0.80–2.52% in the 1-h group compared with 0.78% in control (Fig. S7b), and 1.56–2.24% in the 5-h group compared with 0.46% in control (Fig. 7b). The ratios of cells in anaphase and telophase reduced to 0.00–1.80% in the STLC group compared with 2.24% in control (Fig. 7c). Taken together, the short-term inhibition of Eg5 slightly impairs the transition from metaphase to anaphase.

Consistent with the results of long-term inhibition, we found three types of abnormalities during metaphase, including the abnormal spindle in prometaphase, the asymmetric spindle, and the monoastral spindle (Fig. 7a, Fig. S7a). The ratios of abnormal cells dramatically increased to 0.80–1.51% in 1 h compared with 0.00% in control (Fig. S7d) and increased to 1.03–1.93% in the 5-h group compared with 0.00% in control (Fig. 7d). Compared with long-term inhibition of Eg5, the short-term inhibition results in slighter effects of metaphase-arrested cells and fewer abnormalities of spindle microtubules during metaphase.

Discussion

The distribution pattern of Eg5 proteins on spindle microtubules in dividing spermatocytes

In this study, we have presented the expression pattern of Eg5 proteins in mouse spermatogenic cells using immunofluorescence. We have found that Eg5 proteins mainly accumulated at the spindle poles in spermatocytes during prometaphase and gradually enriched at spindle

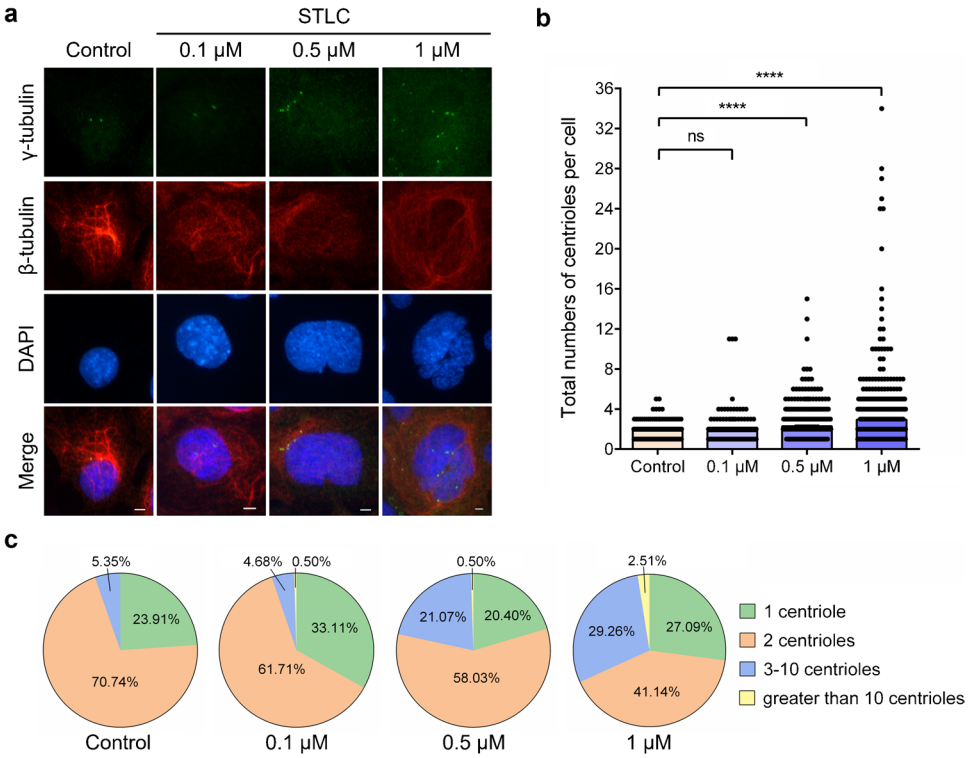

Fig. 6 Eg5 inhibition caused the increased number of centrioles of the GC-2 spd cells. **a** Immunofluorescence images of interphase cells in the control, 0.1, 0.5, and 1 μM STLC groups for 5 days. β-tubulin (red), γ-tubulin (green), and DAPI (blue). Scale bar, 5 μm. **b** Total number of the centrioles per cell in each group was shown (control, 1.83 ± 0.02; 0.1 μM, 1.78 ± 0.04; 0.5 μM, 2.29 ± 0.06; 1 μM, 2.95 ± 0.14). $n = 598$ per group. **c** Ratios of cells with different number of centrioles in the control, 0.1, 0.5, and 1 μM STLC groups. $n = 598$ per group. Student's t test. Error bars, mean ± SEM. ns, $P > 0.05$; ****, $P < 0.0001$

microtubules in spermatocytes during metaphase. Eg5 proteins were reported to be expressed in premeiotic germ cells, including the spermatogonia and spermatocytes (Hara-Yokoyama et al. 2019). We have shown that Eg5 proteins mainly localized at spindle microtubules in dividing spermatocytes at metaphase I. Taken together, these results indicate that Eg5 proteins might play a role in the cell division of spermatocytes.

The localization of Eg5 is corresponding to its functions in cells. We have found that Eg5 proteins were accumulated at the spindle poles in prophase and then distributed along spindle microtubules in cultured GC-2 spd cells. In *Xenopus* eggs, Eg5 proteins are localized at spindle microtubules and mainly enriched near spindle poles (Sawin et al. 1992). The localization of Eg5 proteins at spindle microtubules is important for the crosslinking and sliding of the antiparallel microtubules (Kapitein et al. 2005). Furthermore, in yeast, the enrichment of kinesin-5 Cin8 motors at microtubule minus ends is found to be required for the switch to plus-end-directed motility (Roostalu et al. 2011; Shapira et al. 2017). Bidirectional behaviors of kinesin-5 motors are critical for bipolar spindle formation (Blackwell et al. 2017; Singh et al. 2018). Therefore, the dynamics of evolutionarily conserved Eg5 proteins suggest the different functions of Eg5 proteins in prophase and metaphase during the cell division of spermatocytes.

Eg5 is essential for cell cycle progression and centrosome separation in the spermatocytes

In this study, we have shown that Eg5 inhibition resulted in cell cycle arrest of spermatocytes in metaphase I in vivo. We have revealed that Eg5 inhibition also led to metaphase arrest of the cultured GC-2 spd cells in vitro. Consistent with previous studies, in HeLa cells, STLC treatment results in the specific block in mitotic progression and cell cycle arrest at metaphase (Skoufias et al. 2006). In porcine oocytes, Eg5 inhibition leads to meiotic arrest and cell cycle arrest (Wan et al. 2018). Inhibition or mutation of kinesin-5 leads to the defects in spindle pole separation, spindle collapse, and the formation of the monopolar spindle (Saunders and Hoyt 1992; Sawin et al. 1992; Sharp et al. 1999; Kapoor et al. 2000). Our cell cycle analyses indicate that the spermatocytes are arrested at the G_2/M phase after Eg5 inhibition, which suggests cell cycle progression of the spermatocytes are regulated by kinesin-5 Eg5. Taken together, these findings reveal that kinesin-5 Eg5 is essential for the cell cycle progression of both mitotic and meiotic cells.

Previous studies have established that kinesin-5 motors crosslink antiparallel microtubules and mediate bipolar spindle assembly in mitotic cells (Kapitein et al. 2005; Ferenz et al. 2010). Inhibition of Eg5, by either mutation, siRNA knockdown, or small molecule inhibitors, leads to the failures in spindle pole separation and the formation of

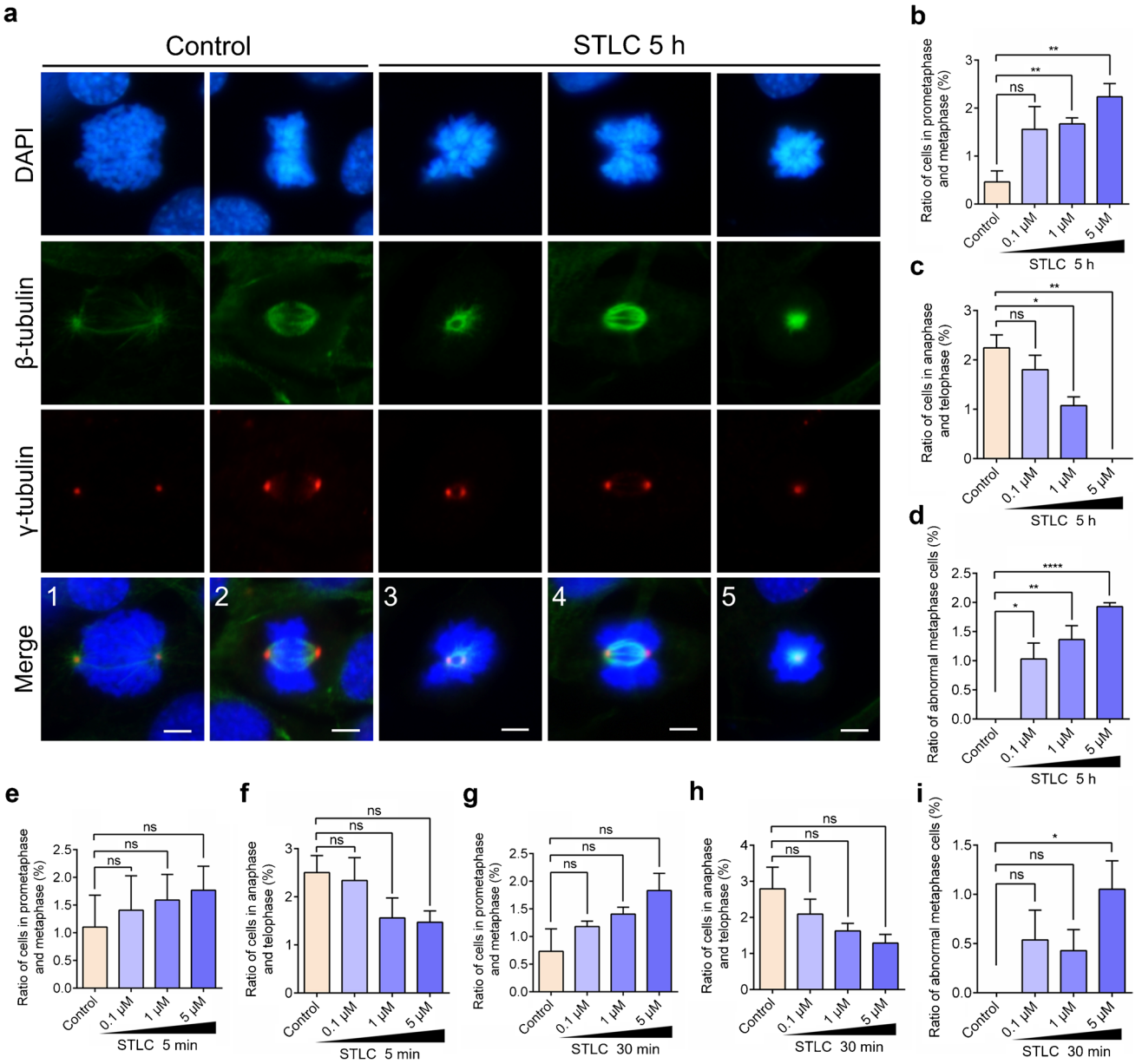

Fig. 7 Short-term inhibition of Eg5 proteins resulted in slight abnormalities during prometaphase and metaphase. **a** Representative images of GC-2 cells after incubating with STLC for 5 h. The control cells in prometaphase (1) and metaphase (2) were shown. There were three main deformities including the abnormal spindle in prometaphase (3), the asymmetric spindle (4), and the monoastral spindle (5). γ-tubulin (red), β-tubulin (green), and DAPI (blue). Scale bar, 5 μm. **b** The ratios of cells in prometaphase and metaphase in the control and 5 h STLC groups were shown (control, 0.46 ± 0.23%; 0.1 μM, 1.56 ± 0.47%; 1 μM, 1.67 ± 0.13%; 5 μM, 2.24 ± 0.28%). $n = 3$ per group. **c** The ratios of cells in anaphase and telophase in the control and 5 h STLC groups were shown (control, 2.24 ± 0.26%; 0.1 μM, 1.80 ± 0.29%; 1 μM, 1.08 ± 0.18%; 5 μM, 0.00 ± 0.00%). $n = 3$ per group. **d** The ratios of abnormal metaphase in the control and 5 h STLC groups were shown (control, 0.00 ± 0.00%; 0.1 μM, 1.03 ± 0.27%; 1 μM, 1.37 ± 0.24%; 5 μM, 1.93 ± 0.07%). $n = 3$ per group. **e** The ratios of cells in prometaphase and metaphase in the control and 5 min STLC groups were shown (control, 1.10 ± 0.57%; 0.1 μM, 1.41 ± 0.62%; 1 μM, 1.59 ± 0.46%; 5 μM, 1.77 ± 0.43%). $n = 3$ per group. **f** The ratios of cells in anaphase and telophase in the control and 5 min STLC groups were shown (control, 2.50 ± 0.35%; 0.1 μM, 2.34 ± 0.47%; 1 μM, 1.56 ± 0.42%; 5 μM, 1.47 ± 0.24%). $n = 3$ per group. **g** The ratios of cells in prometaphase and metaphase in the control and 30 min STLC groups were shown (control, 0.73 ± 0.41%; 0.1 μM, 1.18 ± 0.10%; 1 μM, 1.41 ± 0.12%; 5 μM, 1.83 ± 0.31%). $n = 3$ per group. **h** The ratio of cells in anaphase and telophase in the control and 30-min STLC groups was shown (control, 2.79 ± 0.60%; 0.1 μM, 2.09 ± 0.42%; 1 μM, 1.63 ± 0.21%; 5 μM, 1.29 ± 0.24%). $n = 3$ per group. **I** The ratios of abnormal metaphase in the control and 30 min STLC groups were shown (control, 0.00 ± 0.00%; 0.1 μM, 0.54 ± 0.30%; 1 μM, 0.43 ± 0.21%; 5 μM, 1.05 ± 0.29%). $n = 3$ per group. Error bars, mean ± SEM. ns, $P > 0.05$; *, $P < 0.05$; **, $P < 0.01$; ****, $P < 0.0001$

monopolar spindles (Mayer et al. 1999; Sharp et al. 1999; Kapoor et al. 2000; Mann and Wadsworth 2019). Our previous results have shown that Eg5 is essential for spindle bipolarity and the maintenance of meiotic spindles in the male meiotic division (She et al. 2020). Our present study further explores the specific processes and molecular mechanisms of Eg5 participating in centrosome separation. In this study, we have demonstrated that Eg5 is essential for centrosome separation in dividing spermatocytes. We performed both the short-term and long-term inhibition of Eg5 in the spermatocytes. Eg5 inhibition results in spindle collapse and the significantly increased monopolar spindle in the GC-2 spd cells, as well as in spermatocytes in vivo. Our present study has demonstrated that Eg5 is the principal force generator in centrosome separation in dividing spermatocytes.

Enrichment of Eg5 proteins at the centrosomes is the initial step of the centrosome separation processes. Eg5 proteins act as bipolar homotetramers with the motors at the opposite ends, which is required for the crosslink of adjacent microtubules (Kashina et al. 1997; Scholey et al. 2014). Eg5 tetramers crosslink and slide antiparallel microtubules to regulate bipolar spindle assembly (Sawin et al. 1992; Kapitein et al. 2005). Moreover, the accumulation of Eg5 proteins at microtubules minus ends may be critical for spindle pole separation through the increased interactions between antiparallel microtubules (Mann and Wadsworth 2019). Our data indicate the separation of centrosomes in spermatocytes and the formation of the bipolar spindle is mainly regulated by Eg5 proteins. Overall, whether and how Eg5 interacts with other centrosome-associated proteins to regulate centrosome separation and spindle organization around spindle poles is an outstanding issue that needs to be addressed in the future.

Eg5 contributes to the maintenance of centrosome numbers in spermatocytes

Compared with our previous findings (She et al. 2020), our surprising observations made in this study were the significantly increased numbers of the centrosomes in the GC-2 spd cells by long-term inhibition of Eg5 for 5 days. In most animal cells, the centrosome is the main microtubule organization center (Agircan et al. 2014). Kinesin-5 motors are demonstrated to be the main regulators in the separation of two centrosomes at the onset of cell division (Sawin et al. 1992; Kapoor et al. 2000; Stiff et al. 2020). Centrosome numbers are restricted to one at the G_1/S phase and amplified to two in the G_2/M phase (Godinho 2014).

In contrast, we have found that a portion of the GC-2 spd cells contained excessive centrioles in one single cell. Thus, these results suggest that cell cycle progression is inhibited after Eg5 inhibition, but centrosome amplification was not suppressed in the GC-2 spd cells. Our previous studies have shown that Eg5 inhibition results in monopolar spindles and spindle abnormality in cultured GC-2 spd cells (She et al. 2020). In this study, we further explore the detailed processes and specific mechanisms of centrosome separation regulated by Eg5 in spermatocytes. Interestingly, we observed that there is a significant amplification in the numbers of the centrosomes in cultured spermatocytes, which finally leads to the disorganization of spindle microtubules in these polyploidy cells. Furthermore, the cultured spermatocytes showed large nuclei, multiple nuclei, and cell cycle arrested in interphase after long-term inhibition of Eg5, which indicates the remarkable chromosomal instability and the increase of polyploidy cells.

Previous studies have indicated that Eg5 inhibition results in mitotic arrest and then mitotic apoptosis (Mayer et al. 1999; Ferenz et al. 2010; Shu et al. 2019). However, a portion of cells can undergo mitotic slippage to the next G_1 phase and proceed through the cell cycle as aneuploid or polyploid cells (Ganem et al. 2007; Asraf et al. 2015; Ohashi 2015). In this study, we have shown that cultured spermatocytes showed large nuclei and multiple nuclei in interphase after long-term inhibition of Eg5, which suggests chromosomal instability and the increase of polyploidy cells. Cells with large nuclei and multiple centrosomes in interphase indicate that a portion of the spermatocytes proceeds through the cell cycle by mitotic slippage after Eg5 inhibition. The monopolar spindle formation results in the polyploid cells through the failure in cytokinesis, which might contribute to cell survival and large nuclei (Ohashi 2015).

Eg5 regulates bipolar spindle assembly and chromosome alignment in spermatocytes

Furthermore, our results suggest that Eg5 inhibition significantly reduces the relative distances between the spindle poles in the cultured spermatocytes. Thus, we have demonstrated that Eg5 is required for the control of spindle length in mouse spermatocytes. Kinesin-5 motors generate the outward pushing forces to antagonize the inward pulling forces mediated by kinesin-14 motors or dynein (Kashina et al. 1996; Kapitein et al. 2005; Rincon et al. 2017). Force balances between kinesin-5 and kinesin-14 motors are responsible for bipolar spindle organization and the regulation of spindle length (Fink et al. 2009; Hentrich and Surrey 2010; She and Yang 2017).

In *Drosophila* oocytes, kinesin-5 Klp61F is essential for the maintenance of the bipolar spindle during metaphase I arrest (Wilson et al. 2004; Costa and Ohkura 2019). The changes of kinesin-5's localization from the spindle poles to the equators indicate the distinct functions of kinesin-5 motors at different stages (Costa and Ohkura 2019), which is similar to our observations in mouse spermatocytes. A recent study suggests that kinesin-5 and dynein regulate

the rigid filament assembly and mechanical heterogeneity of the spindle (Takagi et al. 2019), which is corresponding to its localization and the ability to crosslink parallel microtubules (Kapitein et al. 2005; Shimamoto et al. 2015; Tan et al. 2018).

Kinesin-5 motors are important for the maintenance of spindle bipolarity in budding yeast, *Drosophila* and *Xenopus* eggs (Kapoor et al. 2000; Saunders and Hoyt 1992; Sharp et al. 1999). However, in mammalian cells, the metaphase spindles remain bipolar following Eg5 inhibition (Cameron et al. 2006; Ferenz et al. 2009). The resistance to spindle collapse is fulfilled by the functions of kinesin-12 KIF15 (Tanenbaum et al. 2009; Vanneste et al. 2009; Sturgill and Ohi 2013; Sturgill et al. 2016). In addition, Eg5 inhibition also reduces chromosome oscillations in metaphase, which can be rescued by the co-depletion of KIF15 (Vladimirou et al. 2013). Our data indicate that Eg5 is indispensable for the maintenance of bipolar spindle in mouse spermatocytes. However, whether Eg5 and KIF15 function redundantly in the cell division of spermatocytes requires further investigations.

In this study, we demonstrate that Eg5 is responsible for the accurate alignment of chromosomes around the spindle equator in spermatocytes. Eg5 inhibition results in chromosome misalignment in the GC-2 spd cells and finally contributes to chromosomal instability and the increase of polyploidy cells. In yeast, kinesin-5 regulates chromosome congression at the spindle equator (Gardner et al. 2008; McCoy et al. 2015). In *Drosophila* S2 cells, kinesin-5 *Klp61F* knockdown results in longer kinetochore microtubules, less congressed chromosome, and asymmetric chromosome segregation (Tubman et al. 2018). Compared with these organisms, in mammalian cells, the functions of Eg5 in chromosome congression are difficult to observe due to spindle collapse and the formation of monoastral spindles after Eg5 inhibition. Future experiments that solve the problem of inhibiting Eg5 while reducing spindle collapse would define specific mechanisms and molecular networks in chromosome congression of higher eukaryotes.

Eg5 plays a minor role in the organization of the central spindle and midbody in spermatocytes

Eg5 proteins located at the spindle midzone in mitosis (Sharp et al. 1999). We also find that Eg5 proteins are located at the central spindle and gradually accumulate at the midbody in the GC-2 spd cells. In the cultured GC-2 spd cells, STLC-mediated inhibition of Eg5 resulted in the disorganization of the central spindle at anaphase. Eg5 inhibition also disrupted the organization of the midbody and the localization of KIF4A and PRC1 proteins. Our results emphasize the roles of Eg5 in spindle assembly at the late stage of cell division. Eg5 inhibition in anaphase and telophase could lead to mistakes in chromosome segregation, the formation of polyploidy cells, and genome instability in the spermatocytes.

During anaphase, kinesin-5 motors play a role in spindle elongation, but the contributions of kinesin-5 at anaphase are opposite in diverse organisms. In budding yeast, kinesin-5 Cin8 and Kip1 mediate antiparallel microtubule sliding (Movshovich et al. 2008; Gerson-Gurwitz et al. 2009; Roostalu et al. 2011; Fridman et al. 2013). In *D. melanogaster*, kinesin-5 Klp61F regulates spindle pole separation through the sliding forces (Brust-Mascher et al. 2009; Scholey et al. 2016). In contrast, in other systems, kinesin-5 motors generate forces to restrict antiparallel spindle elongation (Collins et al. 2014; Scholey et al. 2016). Inhibition of kinesin-5 motors results in a faster rate of spindle elongation (Saunders et al. 2007; Rozelle et al. 2011; Shimamoto et al. 2015), indicating that kinesin-5 motors function as a molecular brake between antiparallel microtubules. For example, mutations of kinesin-5 in *C. elegans* (Saunders et al. 2007), in *Dictyostelium discoideum* (Tikhonenko et al. 2008), in mammalian LLC-Pk1 cells (Collins et al. 2014) lead to faster spindle elongation. Our results indicate that the crosslinking ability of Eg5 proteins among midzone microtubules might be responsible for the control of spindle elongation.

Conclusion

We have shown that Eg5 locates at spindle poles at prophase and distributes along spindle microtubules at metaphase in dividing spermatocytes. Eg5 proteins are required for cell cycle progression, bipolar spindle assembly, and chromosome alignment in cultured GC-2 spd cells. We have demonstrated that Eg5 inhibition results in spindle collapse, the formation of monopolar spindle, and spindle disorganization in spermatocytes. Furthermore, Eg5 regulates the separation of centrosomes in the early prophase and also mediates the distances of the spindle poles, which finally contribute to the organization of bipolar spindle and chromosome alignment. Strikingly, we have revealed that there is a significant increase in centrosome numbers after long-term inhibition of Eg5 in spermatocytes. In addition, our results suggest that Eg5 plays a minor role in microtubule organization in the central spindle and midbody at the late stage of cell division. In conclusion, our results highlight how kinesin-5 Eg5 functions to mediate centrosome separation and regulate spindle assembly in dividing spermatocytes.

Supplementary Information The online version contains supplementary material available at https://doi.org/10.1007/s00412-022-00772-5.

Acknowledgements We thank all the members of the Cytoskeleton Laboratory at Fujian Medical University for helpful discussions. We thank Jun-Jin Lin, Ming-Xia Wu, and Lin-Ying Zhou at Public Technology Service Center, Fujian Medical University, for their technical assistance.

Author contribution ZYS: conceptualization; data curation; formal analysis; funding acquisition; investigation; methodology; project administration; resources; software; supervision; validation; visualization; roles/writing—original draft; writing—review and editing. NZ: data curation; formal analysis; software; validation; visualization; roles/writing—original draft. YLW: formal analysis; visualization; roles/writing—original draft.

Funding This study was supported by the following grants: National Natural Science Foundation of China (grant number 82001608), Natural Science Foundation of Fujian Province, China (grant number 2019J05071), Fujian Provincial Health Technology Project (grant number 2018–1-69 and 2020QNB009), Startup Fund for scientific research, Fujian Medical University (grant number 2017XQ1001), Fujian Medical University high-level talents scientific research start-up funding project (grant number XRCZX2017025), and Research project of online education and teaching of Chinese medicine graduate students (grant number B-YXC20200202-06).

Data availability The data that support the findings of this study are available from the corresponding author upon reasonable request.

Declarations

Ethics approval All procedures performed in the studies involving animals were approved by the Animal Care and Use Committee at Fujian Medical University, China (permit number SYXK2016-0007).

Conflict of interest The authors declare no competing interests.

References

Agircan FG, Schiebel E, Mardin BR (2014) Separate to operate: control of centrosome positioning and separation. Philos Trans R Soc Lond B Biol Sci 369:20130461

Asraf H, Avunie-Masala R, Hershfinkel M, Gheber L (2015) Mitotic slippage and expression of survivin are linked to differential sensitivity of human cancer cell-lines to the Kinesin-5 inhibitor monastrol. PLoS One 10:e0129255

Blackwell R, Edelmaier C, Sweezy-Schindler O, Lamson A, Gergely ZR, O'Toole E, Crapo A, Hough LE, McIntosh JR, Glaser MA et al (2017) Physical determinants of bipolar mitotic spindle assembly and stability in fission yeast. Sci Adv 3:e1601603

Blangy A, Lane HA, d'Hérin P, Harper M, Kress M, Nigg EA (1995) Phosphorylation by p34cdc2 regulates spindle association of human Eg5, a kinesin-related motor essential for bipolar spindle formation in vivo. Cell 83:1159–1169

Bornens M (2002) Centrosome composition and microtubule anchoring mechanisms. Curr Opin Cell Biol 14:25–34

Brier S, Lemaire D, Debonis S, Forest E, Kozielski F (2004) Identification of the protein binding region of S-trityl-L-cysteine, a new potent inhibitor of the mitotic kinesin Eg5. Biochemistry 43:13072–13082

Brust-Mascher I, Sommi P, Cheerambathur DK, Scholey JM (2009) Kinesin-5-dependent poleward flux and spindle length control in Drosophila embryo mitosis. Mol Biol Cell 20:1749–1762

Cameron LA, Yang G, Cimini D, Canman JC, Kisurina-Evgenieva O, Khodjakov A, Danuser G, Salmon ED (2006) Kinesin 5-independent poleward flux of kinetochore microtubules in PtK1 cells. J Cell Biol 173:173–179

Castillo A, Justice MJ (2007) The kinesin related motor protein, Eg5, is essential for maintenance of pre-implantation embryogenesis. Biochem Biophys Res Commun 357:694–699

Chauvière M, Kress C, Kress M (2008) Disruption of the mitotic kinesin Eg5 gene (Knsl1) results in early embryonic lethality. Biochem Biophys Res Commun 372:513–519

Chen H, Connell M, Mei L, Reid GSD, Maxwell CA (2018) The non-motor adaptor HMMR dampens Eg5-mediated forces to preserve the kinetics and integrity of chromosome segregation. Mol Biol Cell 29:786–796

Chen H, Fok KL, Jiang X, Jiang J, Chen Z, Gui Y, Chan HC, Cai Z (2012) CD147 regulates apoptosis in mouse spermatocytes but not spermatogonia. Hum Reprod 27:1568–1576

Chimento A, Sirianni R, Casaburi I, Ruggiero C, Maggiolini M, Andò S, Pezzi V (2012) 17β-Estradiol activates GPER- and ESR1-dependent pathways inducing apoptosis in GC-2 cells, a mouse spermatocyte-derived cell line. Mol Cell Endocrinol 355:49–59

Collins E, Mann BJ, Wadsworth P (2014) Eg5 restricts anaphase B spindle elongation in mammalian cells. Cytoskeleton (Hoboken) 71:136–144

Costa MFA, Ohkura H (2019) The molecular architecture of the meiotic spindle is remodeled during metaphase arrest in oocytes. J Cell Biol 218:2854–2864

DeBonis S, Skoufias DA, Lebeau L, Lopez R, Robin G, Margolis RL, Wade RH, Kozielski F (2004) In vitro screening for inhibitors of the human mitotic kinesin Eg5 with antimitotic and antitumor activities. Mol Cancer Ther 3:1079–1090

Ferenz NP, Gable A, Wadsworth P (2010) Mitotic functions of kinesin-5. Semin Cell Dev Biol 21:255–259

Ferenz NP, Paul R, Fagerstrom C, Mogilner A, Wadsworth P (2009) Dynein antagonizes eg5 by crosslinking and sliding antiparallel microtubules. Curr Biol 19:1833–1838

Fink G, Hajdo L, Skowronek KJ, Reuther C, Kasprzak AA, Diez S (2009) The mitotic kinesin-14 Ncd drives directional microtubule-microtubule sliding. Nat Cell Biol 11:717–723

Fridman V, Gerson-Gurwitz A, Shapira O, Movshovich N, Lakämper S, Schmidt CF, Gheber L (2013) Kinesin-5 Kip1 is a bi-directional motor that stabilizes microtubules and tracks their plus-ends in vivo. J Cell Sci 126:4147–4159

Ganem NJ, Storchova Z, Pellman D (2007) Tetraploidy, aneuploidy and cancer. Curr Opin Genet Dev 17:157–162

Gardner MK, Bouck DC, Paliulis LV, Meehl JB, O'Toole ET, Haase J, Soubry A, Joglekar AP, Winey M, Salmon ED et al (2008) Chromosome congression by Kinesin-5 motor-mediated disassembly of longer kinetochore microtubules. Cell 135:894–906

Gartner M, Sunder-Plassmann N, Seiler J, Utz M, Vernos I, Surrey T, Giannis A (2005) Development and biological evaluation of potent and specific inhibitors of mitotic Kinesin Eg5. ChemBioChem 6:1173–1177

Gayek AS, Ohi R (2014) Kinetochore-microtubule stability governs the metaphase requirement for Eg5. Mol Biol Cell 25:2051–2060

Gerson-Gurwitz A, Movshovich N, Avunie R, Fridman V, Moyal K, Katz B, Hoyt MA, Gheber L (2009) Mid-anaphase arrest in S. cerevisiae cells eliminated for the function of Cin8 and dynein. Cell Mol Life Sci 66:301–313

Godinho SA (2014) Centrosome amplification and cancer: branching out. Mol Cell Oncol 2:e993252

Hara-Yokoyama M, Kurihara H, Ichinose S, Matsuda H, Ichinose S, Kurosawa M, Tada N, Iwahara C, Terasawa K, Podyma-Inoue KA et al (2019) KIF11 as a potential marker of spermatogenesis within mouse seminiferous tubule cross-sections. J Histochem Cytochem 67:813–824

Hashimoto K, Chinen T, Kitagawa D (2020) Mechanisms of spindle bipolarity establishment in acentrosomal human cells. Mol Cell Oncol 7:1743899

Heck MM, Pereira A, Pesavento P, Yannoni Y, Spradling AC, Goldstein LS (1993) The kinesin-like protein KLP61F is essential for mitosis in Drosophila. J Cell Biol 123:665–679

Hentrich C, Surrey T (2010) Microtubule organization by the antagonistic mitotic motors kinesin-5 and kinesin-14. J Cell Biol 189:465–480

Hofmann MC, Abramian D, Millán JL (1995) A haploid and a diploid cell coexist in an in vitro immortalized spermatogenic cell line. Dev Genet 16:119–127

Hofmann MC, Hess RA, Goldberg E, Millán JL (1994) Immortalized germ cells undergo meiosis in vitro. Proc Natl Acad Sci U S A 91:5533–5537

Iwakiri Y, Kamakura S, Hayase J, Sumimoto H (2013) Interaction of NuMA protein with the kinesin Eg5: its possible role in bipolar spindle assembly and chromosome alignment. Biochem J 451:195–204

Kaan HY, Ulaganathan V, Hackney DD, Kozielski F (2009) An allosteric transition trapped in an intermediate state of a new kinesin-inhibitor complex. Biochem J 425:55–60

Kapitein LC, Peterman EJ, Kwok BH, Kim JH, Kapoor TM, Schmidt CF (2005) The bipolar mitotic kinesin Eg5 moves on both microtubules that it crosslinks. Nature 435:114–118

Kapoor TM, Mayer TU, Coughlin ML, Mitchison TJ (2000) Probing spindle assembly mechanisms with monastrol, a small molecule inhibitor of the mitotic kinesin, Eg5. J Cell Biol 150:975–988

Kashina AS, Rogers GC, Scholey JM (1997) The bimC family of kinesins: essential bipolar mitotic motors driving centrosome separation. Biochim Biophys Acta 1357:257–271

Kashina AS, Scholey JM, Leszyk JD, Saxton WM (1996) An essential bipolar mitotic motor. Nature 384:225

Kovacovicova K, Awadova T, Mikel P, Anger M (2016) In vitro maturation of mouse oocytes increases the level of Kif11/Eg5 on meiosis II spindles. Biol Reprod 95:18

Leblond CP, Clermont Y (1952a) Definition of the stages of the cycle of the seminiferous epithelium in the rat. Ann N Y Acad Sci 55:548–573

Leblond CP, Clermont Y (1952b) Spermiogenesis of rat, mouse, hamster and guinea pig as revealed by the periodic acid-fuchsin sulfurous acid technique. Am J Anat 90:167–215

Liu M, Li D, Sun L, Chen J, Sun X, Zhang L, Huo L, Zhou J (2014) Modulation of Eg5 activity contributes to mitotic spindle checkpoint activation and Tat-mediated apoptosis in CD4-positive T-lymphocytes. J Pathol 233:138–147

Ma N, Titus J, Gable A, Ross JL, Wadsworth P (2011) TPX2 regulates the localization and activity of Eg5 in the mammalian mitotic spindle. J Cell Biol 195:87–98

Mann BJ, Wadsworth P (2019) Kinesin-5 regulation and function in mitosis. Trends Cell Biol 29:66–79

Mayer TU, Kapoor TM, Haggarty SJ, King RW, Schreiber SL, Mitchison TJ (1999) Small molecule inhibitor of mitotic spindle bipolarity identified in a phenotype-based screen. Science 286:971–974

McCoy KM, Tubman ES, Claas A, Tank D, Clancy SA, O'Toole ET, Berman J, Odde DJ (2015) Physical limits on kinesin-5-mediated chromosome congression in the smallest mitotic spindles. Mol Biol Cell 26:3999–4014

Movshovich N, Fridman V, Gerson-Gurwitz A, Shumacher I, Gertsberg I, Fich A, Hoyt MA, Katz B, Gheber L (2008) Slk19-dependent mid-anaphase pause in kinesin-5-mutated cells. J Cell Sci 121:2529–2539

Novak M, Polak B, Simunić J, Boban Z, Kuzmić B, Thomae AW, Tolić IM, Pavin N (2018) The mitotic spindle is chiral due to torques within microtubule bundles. Nat Commun 9:3571

Ohashi A (2015) Different cell fates after mitotic slippage: from aneuploidy to polyploidy. Mol Cell Oncol 3:e1088503

Raaijmakers JA, van Heesbeen RG, Meaders JL, Geers EF, Fernandez-Garcia B, Medema RH, Tanenbaum ME (2012) Nuclear envelope-associated dynein drives prophase centrosome separation and enables Eg5-independent bipolar spindle formation. EMBO J 31:4179–4190

Rincon SA, Lamson A, Blackwell R, Syrovatkina V, Fraisier V, Paoletti A, Betterton MD, Tran PT (2017) Kinesin-5-independent mitotic spindle assembly requires the antiparallel microtubule crosslinker Ase1 in fission yeast. Nat Commu 8:15286

Roostalu J, Hentrich C, Bieling P, Telley IA, Schiebel E, Surrey T (2011) Directional switching of the kinesin Cin8 through motor coupling. Science 332:94–99

Rozelle DK, Hansen SD, Kaplan KB (2011) Chromosome passenger complexes control anaphase duration and spindle elongation via a kinesin-5 brake. J Cell Biol 193:285–294

Russell LD, Ettlin RA, Hikim APS, Clegg ED (1990) Histological and histopathological evaluation of the testis. Cache River Press, Florida, pp 119–162

Saunders AM, Powers J, Strome S, Saxton WM (2007) Kinesin-5 acts as a brake in anaphase spindle elongation. Curr Biol 17:R453–R454

Saunders WS, Hoyt MA (1992) Kinesin-related proteins required for structural integrity of the mitotic spindle. Cell 70:451–458

Sawin KE, LeGuellec K, Philippe M, Mitchison TJ (1992) Mitotic spindle organization by a plus-end-directed microtubule motor. Nature 359:540–543

Scholey JE, Nithianantham S, Scholey JM, Al-Bassam J (2014) Structural basis for the assembly of the mitotic motor Kinesin-5 into bipolar tetramers. Elife 3:e02217

Scholey JM, Civelekoglu-Scholey G, Brust-Mascher I (2016) Anaphase B. Biology (Basel) 5:51

Shapira O, Goldstein A, Al-Bassam J, Gheber L (2017) A potential physiological role for bi-directional motility and motor clustering of mitotic kinesin-5 Cin8 in yeast mitosis. J Cell Sci 130:725–734

Sharp DJ, McDonald KL, Brown HM, Matthies HJ, Walczak C, Vale RD, Mitchison TJ, Scholey JM (1999) The bipolar kinesin, KLP61F, cross-links microtubules within interpolar microtubule bundles of Drosophila embryonic mitotic spindles. J Cell Biol 144:125–138

She ZY, Yang WX (2017) Molecular mechanisms of kinesin-14 motors in spindle assembly and chromosome segregation. J Cell Sci 130:2097–2110

She ZY, Zhong N, Yu KW, Xiao Y, Wei YL, Lin Y, Li YL, Lu MH (2020) Kinesin-5 Eg5 is essential for spindle assembly and chromosome alignment of mouse spermatocytes. Cell Div 15:6

Shimamoto Y, Forth S, Kapoor TM (2015) Measuring pushing and braking forces generated by ensembles of Kinesin-5 crosslinking two microtubules. Dev Cell 34:669–681

Shimizu M, Ishii H, Ogo N, Matsuno K, Asai A (2010) Biochemical analysis of cellular target of S-trityl-L-cysteine derivatives using affinity matrix. Bioorg Med Chem Lett 20:1578–1580

Shu S, Iimori M, Wakasa T, Ando K, Saeki H, Oda Y, Oki E, Maehara Y (2019) The balance of forces generated by kinesins controls spindle polarity and chromosomal heterogeneity in tetraploid cells. J Cell Sci 132:jcs231530

Singh SK, Pandey H, Al-Bassam J, Gheber L (2018) Bidirectional motility of kinesin-5 motor proteins: structural determinants, cumulative functions and physiological roles. Cell Mol Life Sci 75:1757–1771

Skoufias DA, DeBonis S, Saoudi Y, Lebeau L, Crevel I, Cross R, Wade RH, Hackney D, Kozielski F (2006) S-trityl-L-cysteine is a reversible, tight binding inhibitor of the human kinesin Eg5 that specifically blocks mitotic progression. J Biol Chem 281:17559–17569

Stiff T, Echegaray-Iturra FR, Pink HJ, Herbert A, Reyes-Aldasoro CC, Hochegger H (2020) Prophase-specific perinuclear actin coordinates centrosome separation and positioning to ensure accurate chromosome segregation. Cell Rep 31:107681

Sturgill EG, Norris SR, Guo Y, Ohi R (2016) Kinesin-5 inhibitor resistance is driven by kinesin-12. J Cell Biol 213:213–227

Sturgill EG, Ohi R (2013) Kinesin-12 differentially affects spindle assembly depending on its microtubule substrate. Curr Biol 23:1280–1290

Takagi J, Sakamoto R, Shiratsuchi G, Maeda YT, Shimamoto Y (2019) Mechanically distinct microtubule arrays determine the length and force response of the meiotic spindle. Dev Cell 49:267-278.e5

Tan R, Foster PJ, Needleman DJ, McKenney RJ (2018) Cooperative accumulation of dynein-dynactin at microtubule minus-ends drives microtubule network reorganization. Dev Cell 44:233-247.e4

Tanenbaum ME, Macůrek L, Janssen A, Geers EF, Alvarez-Fernández M, Medema RH (2009) Kif15 cooperates with eg5 to promote bipolar spindle assembly. Curr Biol 19:1703–1711

Tanenbaum ME, Medema RH (2010) Mechanisms of centrosome separation and bipolar spindle assembly. Dev Cell 19:797–806

Tikhonenko I, Nag DK, Martin N, Koonce MP (2008) Kinesin-5 is not essential for mitotic spindle elongation in Dictyostelium. Cell Motil Cytoskeleton 65:853–862

Tubman E, He Y, Hays TS, Odde DJ (2018) Kinesin-5 mediated chromosome congression in insect spindles. Cell Mol Bioeng 11:25–36

van Heesbeen RG, Tanenbaum ME, Medema RH (2014) Balanced activity of three mitotic motors is required for bipolar spindle assembly and chromosome segregation. Cell Rep 8:948–956

Vanneste D, Takagi M, Imamoto N, Vernos I (2009) The role of Hklp2 in the stabilization and maintenance of spindle bipolarity. Curr Biol 19:1712–1717

Vladimirou E, Mchedlishvili N, Gasic I, Armond JW, Samora CP, Meraldi P, McAinsh AD (2013) Nonautonomous movement of chromosomes in mitosis. Dev Cell 27:60–71

Wan X, Zhang Y, Lan M, Pan MH, Tang F, Zhang HL, Ou XH, Sun SC (2018) Meiotic arrest and spindle defects are associated with altered KIF11 expression in porcine oocytes. Environ Mol Mutagen 59:805–812

Wilson PG, Simmons R, Saighal S (2004) Novel nuclear defects in KLP61F-deficient mutants in Drosophila are partially suppressed by loss of Ncd function. J Cell Sci 117:4921–4933

Xie Y, Cheng M, Lu S, Yuan Q, Yang D, Chen Y, Pan C, Qiu Y, Xiong B (2018) Eg5 orchestrates porcine oocyte maturational progression by maintaining meiotic organelle arrangement. Cell Div 13:4

Yount AL, Zong H, Walczak CE (2015) Regulatory mechanisms that control mitotic kinesins. Exp Cell Res 334:70–77

Yukawa M, Yamada Y, Toda T (2019) Suppressor analysis uncovers that MAPs and microtubule dynamics balance with the Cut7/Kinesin-5 motor for mitotic spindle assembly in Schizosaccharomyces pombe. G3 (Bethesda) 9:269–280

Zhang J, Liu J, Ren L, Wei J, Zhang F, Li Y, Guo C, Duan J, Sun Z, Zhou X (2018) Silica nanoparticles induce abnormal mitosis and apoptosis via PKC-δ mediated negative signaling pathway in GC-2 cells of mice. Chemosphere 208:942–950